Reactive transport of chemicals in compacted bentonite under nonisothermal water infiltration

Sedighi, Majid; Thomas, Hywel R.; Vardon, Philip J.

DOI
10.1061/(ASCE)GT.1943-5606.0001955

Publication date
2018

Document Version
Final published version

Published in
Journal of Geotechnical and Geoenvironmental Engineering

Citation (APA)
Sedighi, M., Thomas, H. R., & Vardon, P. J. (2018). Reactive transport of chemicals in compacted bentonite under nonisothermal water infiltration. *Journal of Geotechnical and Geoenvironmental Engineering*, *144*(10), Article 04018075. https://doi.org/10.1061/(ASCE)GT.1943-5606.0001955

Reactive Transport of Chemicals in Compacted Bentonite under Nonisothermal Water Infiltration

Majid Sedighi[1]; Hywel R. Thomas[2]; and Philip J. Vardon[3]

Abstract: This paper presents an investigation of coupled thermal, hydraulic, and chemical behavior of a compacted bentonite buffer under the heating and hydration conditions of geological disposal of high-level nuclear waste. The study presented provides further insight into the evolution of hydro-geochemistry of the compacted bentonite and the clay microstructure effects through a numerical modelling development of the reactive transport of multicomponent chemicals. The application/validation case study is based on a series of laboratory tests on heating and hydration of compacted bentonite for a period of 0.5–7.6 years reported in the literature. The effects of microstructure evolution during hydration and dehydration on the transport phenomena are included via a new approach that links the geochemistry of clay hydration/dehydration with the transport properties. The analysis results related to the moisture flow and chloride transport demonstrate close correlation with the experimental results by the inclusion of the effects of microstructure evolution in the transport phenomena. The results of numerical analysis of reactive transport of chemicals highlight the importance of accessory minerals present in bentonite on the distribution of some anionic species. The behavior of major cationic species is shown to be mainly governed by the transport processes. Further insights into the chemically driven processes in clay buffer due to coupled hydraulic and thermal effects are presented and discussed that are captured from the results of modeling the clay-water-chemical system. **DOI: 10.1061/(ASCE)GT.1943-5606.0001955.**

Author keywords: Compacted bentonite; Reactive transport; Coupled behavior; Hydro-geochemistry; Clay microstructure.

Introduction

The application of swelling clays in a compacted form is envisaged as a key component of the engineered barrier system (EBS) in geological concepts for the disposal of high level radioactive waste (HLW). It has been shown that the engineering behavior of compacted swelling clays is strongly coupled with the hydro-geochemical processes that can occur in the clay-water-chemical system (e.g., Pusch and Yong 2006; Steefel et al. 2010). Under variable thermal, hydraulic, and chemical environment of the geological repository, geochemical interactions between the ionic species, clay, and accessory minerals can induce considerable changes on the physical, chemical, and mechanical behavior of the clay buffer. An in-depth understanding of the multiphase, multicomponent, and interacting hydro-geochemical system of the clay-water and its evolution under chemically-coupled processes is therefore important for the performance assessment of the compacted clay buffer. The study presented here aims to provide further insight into the evolution of hydro-geochemistry of compacted bentonite through coupled modelling of thermal, hydraulic, and chemical processes.

An evolutionary phase in the operational life of the clay buffer under the conditions of the HLW repository starts after the emplacement of the buffer in the depositional holes where the partially saturated compacted bentonite can be exposed to an elevated temperature at the boundary adjacent to the HLW canister (heating) and resaturation at the interface with the host rock (hydration). Considerable attempts have been made over the last three decades or so to study the physical, chemical/geochemical, and mechanical behavior of compacted bentonite buffer under heating and hydration effects through experimental studies at different scales (e.g., Martín et al. 2000; ENRESA 2000; Cuevas et al. 2002; Villar et al. 2008a) and numerical modelling investigations that have been tested against the results of laboratory, mock-up, and in-situ heating and hydration tests (e.g., Guimarães et al. 2007; Cleall et al. 2007; Samper et al. 2008; Zheng and Samper 2008; Villar et al. 2008b; Steefel et al. 2010). There are also numerical modelling studies on the long-term behavior of compacted bentonite as part of the EBS (e.g., Arcos et al. 2008; Yang et al. 2008).

The coupled modelling study presented in this paper is based on a notable series of laboratory-scale heating and hydration tests on compacted FEBEX bentonite reported in the literature (Villar 2007; Villar et al. 2008a, b; Fernández and Villar 2010). The series of heating and hydration experiments described in the preceding have been carried out on cylindrical samples of FEBEX bentonite, compacted at dry density around 1,650 kg/m^3 and tested for periods 0.5, 1, 2, and 7.6 years. Fig. 1 presents a schematic of the heating and hydration experiments whose results have been used. The results of geochemical postmortem hydrogeochemical analysis of the heating and hydration tests have been reported by Villar et al. (2008b) and Fernández and Villar (2010) that provide extensive data and important insight into the evolution of hydro-geochemistry of the compacted bentonite at the end of experiments.

[1]Lecturer, School of Mechanical, Aerospace and Civil Engineering, Univ. of Manchester, Manchester M13 9PL, UK; formerly, Research Fellow, Geoenvironmental Research Centre, Cardiff Univ., Cardiff CF24 3AA, UK (corresponding author). Email: Majid.Sedighi@manchester.ac.uk

[2]Professor, Geoenvironmental Research Centre, School of Engineering, Cardiff Univ., Cardiff CF24 3AA, UK. Email: ThomasHR@cardiff.ac.uk

[3]Associate Professor, Section for Geo-Engineering, Faculty of Civil Engineering and Geosciences, Delft Univ. of Technology, Bldg. 23, Stevinweg 1, P.O. Box 5048, 2628 CN Delft, 2600 GA Delft, Netherlands; formerly, Research Fellow, Geoenvironmental Research Centre, Cardiff Univ., Cardiff CF24 3AA, UK. Email: P.J.Vardon@tudelft.nl

Note. This manuscript was submitted on November 7, 2016; approved on April 26, 2018; published online on August 11, 2018. Discussion period open until January 11, 2019; separate discussions must be submitted for individual papers. This paper is part of the ***Journal of Geotechnical and Geoenvironmental Engineering***, © ASCE, ISSN 1090-0241.

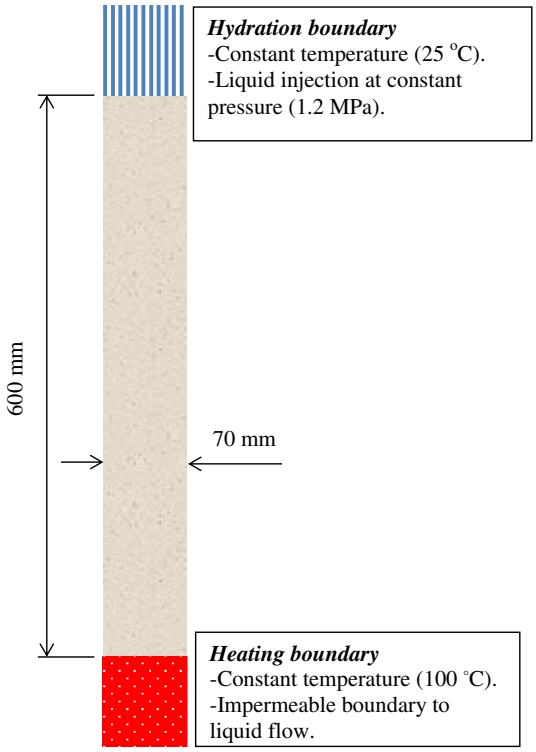

Fig. 1. Heating and hydration experiments. (Data from Villar et al. 2008a.)

However, data presented and knowledge gained is mainly based on the analysis after completion of the tests (i.e., 0.5, 1, 2, and 7.6 years) in which the conditions of the tests were different from the thermal and hydraulic conditions inside the sample (in-situ conditions) during the heating and hydrations. Specifically, the concentration of ionic species have been measured in the laboratory at a solid to liquid ratio of 1:4 and at 20°C, which is different from the in-situ conditions at the end of the tests associated with each slice of the sample.

The numerical modelling and investigation presented aims to (1) provide a more comprehensive understanding of the transient hydro-geochemical processes during the heating and hydration tests on compacted bentonite (hereafter: transient analysis); (2) obtain a better understanding of temporal evolution of the soil-water-chemical system that is not directly possible to obtain from the experimental results; and (3) examine the validity of the numerical model developed and applied against an experimental dataset at the end of the transient analyses considering similar temperature and water content conditions applied in the postmortem experiments (hereafter: postmortem analysis).

An important aspect in the prediction of behavior of a compacted clay buffer is related to the effects of microstructure of bentonite on the flow of water and transport of chemicals (Yong 2003). Comparisons between the results of modelling investigations and experimental data have highlighted the importance of microstructure processes in moisture flow in compacted bentonite (e.g., Thomas et al. 2003; Sánchez et al. 2012; Thomas and Sedighi 2012). Theoretical approaches have been proposed to describe the effects of microstructure deformation (expansion/shrinkage) on hydraulic or hydromechanical behavior of compacted bentonite (e.g., Thomas et al. 2003; Kröhn 2003; Xie et al. 2006; Sánchez et al. 2012; Navarro et al. 2014). The effects of clay-water-chemical interactions are also manifested in the transport of chemicals as experimental studies show that the effective diffusion coefficients of ionic species vary considerably with the type of chemical species in the compacted bentonite (e.g., Kozaki et al. 2001; Muurinen et al. 2007; Van Loon et al. 2007; Wersin et al. 2004). In this study, we consider the effects of a microstructure of compacted bentonite and its evolution on moisture flow and chemical transport. We adopt a new approach proposed by Sedighi and Thomas (2014) by which the hydration and dehydration of microstructure of compacted bentonite and its associated porosity are calculated directly from thermodynamics of hydration/dehydration of smectite.

A summary of the governing formulations and the numerical model is first presented. The procedure of analysis, material properties, initial conditions, and boundary conditions applied in the simulations are discussed in detail. The results of simulations are presented that include two stages of analysis: (1) the transient analysis of evolution of thermal, hydraulic, and chemical/geochemical variables in the domain under the same conditions that have been applied in the heating and hydration tests by Villar et al. (2008b); and (2) the postmortem geochemical analysis of the results from the first stage that are based on the same thermal and hydraulic conditions applied in the geochemical postmortem analysis as reported by Fernández and Villar (2010). The results are compared with those reported from the experimental tests, enabling identification of key hydro-geochemical processes involved during the test and examining the accuracy of the model under the conditions of the application case.

Coupled Thermal, Hydraulic and Chemical Formulations and Numerical Model

The numerical investigation presented was carried out by extending the capabilities and theoretical aspects of a coupled thermal, hydraulic, chemical, and mechanical model (THCM) (COMPASS) (e.g., Thomas and He 1997; Seetharam et al. 2007; Vardon et al. 2011; Sedighi et al. 2016) through (1) development of a theoretical formulation for multicomponent chemical transport under coupled thermohydraulic conditions (Sedighi et al. 2011; Thomas et al. 2012); (2) inclusion of microstructure effects in transport phenomena by developing a chemistry-based microporosity evolution model (Sedighi and Thomas 2014); and (3) integration of the geochemical model PHREEQC into the transport model to form an integrated reactive transport model under coupled THCM formulation (i.e., COMPASS-PHREEQC) (Sedighi et al. 2015; Sedighi et al. 2016).

The processes considered in the governing equations of the model are: (1) heat transfer via conduction, convection, and latent heat of vaporization; (2) moisture (water and vapor) flow due to thermal and hydraulic driving potentials; (3) transport of multicomponent chemicals via advection, dispersion, and diffusion mechanisms; and (4) heterogeneous and homogenous geochemical reactions that can occur in the soil, water, and air system.

Heat Transfer and Moisture Flow

The governing equation for heat transfer considers the energy conservation given as (Thomas and He 1997):

$$\frac{\partial[H_c(T-T_r)\delta V + L\rho_v\theta_a]}{\partial t} = -\delta V\nabla\cdot[-\lambda_T\nabla T + L(\rho_l \mathrm{v_v} + \rho_v \mathrm{v_a}) + A(T-T_r)] \quad (1)$$

where H_c is the heat storage capacity and T and T_r represent temperature and the reference temperature, respectively. Time is represented by t, δV represents the incremental volume, L represents the latent heat of vaporization, and θ_a is the volumetric air (gas) content. The water and vapor density are represented by

ρ_l and ρ_v, respectively, while $\mathbf{v}_v$ represents the vapor velocity and v_a represents air velocity. Thermal conductivity is represented by λ_T and A stands for the sum of the heat convection components. Further details related to heat transfer parameters can be found in Thomas and He (1997).

The governing equation for moisture flow is based on the mass conservation law. The flow of water (liquid) in unsaturated porous medium is explained using Darcy's law and the vapor flow is considered to be driven by diffusion and advection processes (Thomas and He 1997):

$$\frac{\partial(\rho_l\theta_l\delta V)}{\partial t}+\frac{\partial(\rho_v\theta_a\delta V)}{\partial t}=-\delta V\nabla\cdot(\rho_l\mathbf{v}_l+\rho_l\mathbf{v}_v+\rho_v\mathbf{v}_a) \quad (2)$$

where θ_l is the total volumetric liquid content and v_l represents the water velocity.

By considering capillary and gravitational potentials, the liquid flux, in an expanded form, can be written as (Thomas and He 1997):

$$v_l=k_l\left(\frac{\nabla u_l}{\rho_l g}+\nabla z\right) \quad (3)$$

where, k_l is the unsaturated hydraulic conductivity of soil, u_l is the pore water pressure, g is the gravitational constant, and z stands for the elevation.

The diffusive component of the vapor flow is considered based on the formulation proposed by Philip and de Vries (1957):

$$\mathbf{v}_v=\left[\frac{D_{atms}v_v\tau_v(1-\theta_l)}{\rho_l}\rho_0\frac{\partial h}{\partial s}\right]\Delta u_l-\left[\frac{D_{atms}v_v}{\rho_l}f\frac{(\nabla T)a}{\nabla T}\left(h\frac{\partial\rho_0}{\partial T}+\rho_0\frac{\partial h}{\partial T}\right)\right]\nabla T \quad (4)$$

where D_{atms} is the molecular diffusivity of vapor through air, τ_v is the tortuosity factor, v_v is a mass flow factor, ρ_0 is the density of saturated water vapour, h is relative humidity, and s represents total suction. The microscopic pore temperature gradient factor is denoted by $[(\nabla T)_a/\nabla T]$ and f is a flow area factor. The flow factor reduces the vapor flow since the available flow area decreased at higher moisture contents.

Further details related to moisture transfer equations can be found in Sedighi (2011) and Sedighi et al. (2016).

Reactive Transport of Multicomponent Chemicals

The formulations of reactive transport of chemicals are based on mass conservation. The geochemical reactions causing gain or loss of each chemical component are considered via a sink/source term in the transport formulation. The transport formulation considers the transfer mechanisms of advection, diffusion, and dispersion of multiple chemicals in the liquid phase.

It has been shown that anionic and cationic species diffuse at different rates in a multi-ionic aqueous system of compacted smectite. Therefore, the diffusion rate of each ion may deviate from that calculated by Fick's diffusion law (Lasaga 1979). It is therefore required that the condition of electro-neutrality of the aqueous system should be implemented in the transport formulation of multiple ions. Sedighi et al. (2011) and Thomas et al. (2012) have presented a general formulation for chemical transport in multi-ionic systems. The formulation considers diffusion under combined molecular diffusion and thermal diffusion and satisfies the electroneutrality condition of the pore fluid system (a summary of the formulation is presented in Appendix I). It is noted that the formulation only considers flow in the bulk fluid, i.e., the transport of chemicals does not include diffusion via surface diffusion or interlayer diffusion processes.

The mass conservation alongside electroneutrality condition has been adopted to develop the governing equation for the transport:

$$\frac{\partial(\theta_l c_i\delta V)}{\partial t}+\frac{\partial(\theta_l s_i\delta V)}{\partial t}=-\delta V\nabla\cdot\left(c_i\mathbf{v}_l-\sum_{j=1}^{n_c}\theta_l\tau_i D_{ij}\nabla c_j-\theta_l\tau_i D_i^T\nabla T-\mathbf{D}_m\nabla c_j\right) \quad (5)$$

where c_i is the concentration of the i^{th} chemical component and s_i a geochemical sink/source term which stands for the amount of the i^{th} chemical component that is produced or depleted due to geochemical reactions. The effective molecular diffusion coefficient of the i^{th} chemical due to the chemical gradient of the j^{th} chemical component is represented D_{ij}, while D_i^T represents the thermal diffusion coefficient of the i^{th} chemical. The matrix of the effective dispersion coefficients is $\mathbf{D}_m$ and τ_i is the tortuosity factor of the i^{th} chemical component.

The molecular diffusion and thermal diffusion coefficients can be presented as (Thomas et al. 2012):

$$D_{ij}=-\delta_{ij}D_i^0\left(1+\frac{\partial\ln\gamma_i}{\partial\ln c_i}\right)+\frac{z_i D_i^0 c_i}{\sum_{k=1}^{n_c}z_k^2 D_k^0 c_k}Z_j D_j^0\left(1+\frac{\partial\ln\gamma_i}{\partial\ln c_i}\right) \quad (6)$$

$$D_i^T=-D_i^0 c_i\frac{Q_i^{*0}}{RT^2}+\frac{z_i D_i^0 c_i}{\sum_{k=1}^{n_c}z_k^2 D_k^0 c_k}\sum_{j=1}^{n_c}z_j c_j D_j^0\frac{Q_j^{*0}}{RT^2} \quad (7)$$

where δ_{ij} is the Kronecker's delta, D_i^0 is the self-diffusion coefficient of the i^{th} chemical component in free water, z_i stands for the ionic valence of the i^{th} chemical component, and Q_j^{*0} is the heat of transport of the j^{th} chemical component.

The geochemical sink/source term in the governing equation of chemicals are calculated using an external geochemical. This was achieved by coupling the geochemical model PHREEQC version 2 (Parkhurst and Appelo 1999) with the transport model (Sedighi et al. 2016). In relation to the application considered in this work, the geochemical modelling features that were coupled to the transport model and tested include (1) equilibrium reactions, applied to precipitation/dissolution of minerals; (2) kinetically controlled reactions, applied to precipitation/dissolution of minerals; and (3) ion exchange processes, considered under equilibrium conditions.

Numerical Model

The numerical solution to the formulations of the heat transfer, moisture flow, and chemical transport has been achieved by the application of the finite element method and the finite difference method (Thomas and He 1997; Seetharam et al. 2007). The Galerkin weighted residual method has been adopted by which the spatial discretization is developed.

The solution adopted for the reactive transport formulation of chemicals is based on an operator splitting approach in which the governing equations for the transport (and mechanical) formulation and the geochemical reactions are solved sequentially (Steefel and MacQuarrie 1996). The operator splitting approach has been extensively adopted in the development of reactive transport models in various forms including sequential iterative approach (SIA), sequentially noniterative approach (SNIA), and sequentially partly-iterative approach (SPIA). Examples of established reactive transport codes are HYDROGEOCHEM (Yeh and Tripathi 1989), CrunchFlow (Steefel 2009), PHREEQC (Parkhurst and Appelo 1999), THOUGHREACT (Xu et al. 2004), HPx

(Jacques and Šimůnek 2005), and CORE 2D (Samper et al. 2009) that adopt operating splitting approaches and are widely applied in various fields.

In order to couple the chemical transport model and the geochemical reaction model (calculated by PHREEQC version 2), a sequential noniterative approach (SNIA) was adopted. In summary, the chemical transport equations are separately solved at each time step and the concentrations of chemicals calculated are then used for the geochemical modelling using PHREEQC. The values of dissolved chemical concentrations corrected after the geochemical modelling are returned into the transport module for the next step of analysis. The coupled reactive transport model presented here has carefully been tested and verified against several benchmarks that are presented in detail elsewhere (Sedighi et al. 2016). Appendix II provides a description of the numerical and computational aspects of the model.

Case Study and Simulation Details

The case study presented here is based on a series of heating and hydration experiments on FEBEX bentonite, compacted at dry density around 1,650 kg/m^3 reported by Villar et al. (2008a, b) that have been carried out for a period of 0.5–7.6 years. As shown in Fig. 2, the experimental tests included the hydration of compacted clay samples by an aqueous solution from the top of the sample at 1.2 MPa (infiltration pressure) and at ambient temperature (20–30°C) while an elevated temperature has been applied at the bottom of the cell (100 °C). The size of the cylindrical samples was 600 mm (height) and 70 mm (diameter).

An axi-symmetric analysis has been carried out on a discretized domain to 500 unequally sized elements (four-noded axi-symmetric elements). In order to prevent numerical instability and improve the convergence, the first 200 mm in the heating side (bottom) and the hydration side (top) of the sample were discretized into smaller elements (equally sized 1 mm elements). Equally sized 2 mm elements were used in the 200 mm distance in the middle of domain. The maximum time-step allowed in the numerical analysis was 500,000 s. The time steps were allowed to the maximum allowed value by a rate of 1.05. If the convergence criteria are satisfied within a specified numbers of iterations, the time-step was allowed to increase; otherwise, the time-step was reduced to a lower value to achieve convergence.

Geochemical analysis of the pore fluid composition at the initial water content (14% gravimetric) and temperature at 25 °C was carried out using PHREEQC by considering the equilibration of the whole clay-water system with pure water at pH 7.72 and atmospheric CO_2 partial pressure ($PCO_2 \approx 10^{-3.5}$). The quantities of the soluble minerals and exchangeable cation contents of the bentonite were adopted from the average values for the FEBEX bentonite provided by Fernández et al. (2001). Following Fernández et al. (2001), dissolution-precipitation of minerals including calcite, halite, and gypsum and ion exchange reactions was considered in the modelling. The coefficients for exchange reactions reported in ENRESA (2000) were employed. For mineral reactions the database of PHREQQC (phreeqc.dat) was used. A summary of the thermodynamics parameters of mineral dissolution/precipitation and ion exchange reactions is provided in Table 1. The results of geochemical modelling of the pore water composition are presented in Table 2. The chemical composition of the aqueous solution injected to the system is also presented in Table 2.

A coupled thermal, hydraulic, and chemical analysis was carried out to obtain the transient evolution of key variables in the domain that include temperature, pore water pressure, ionic species in the

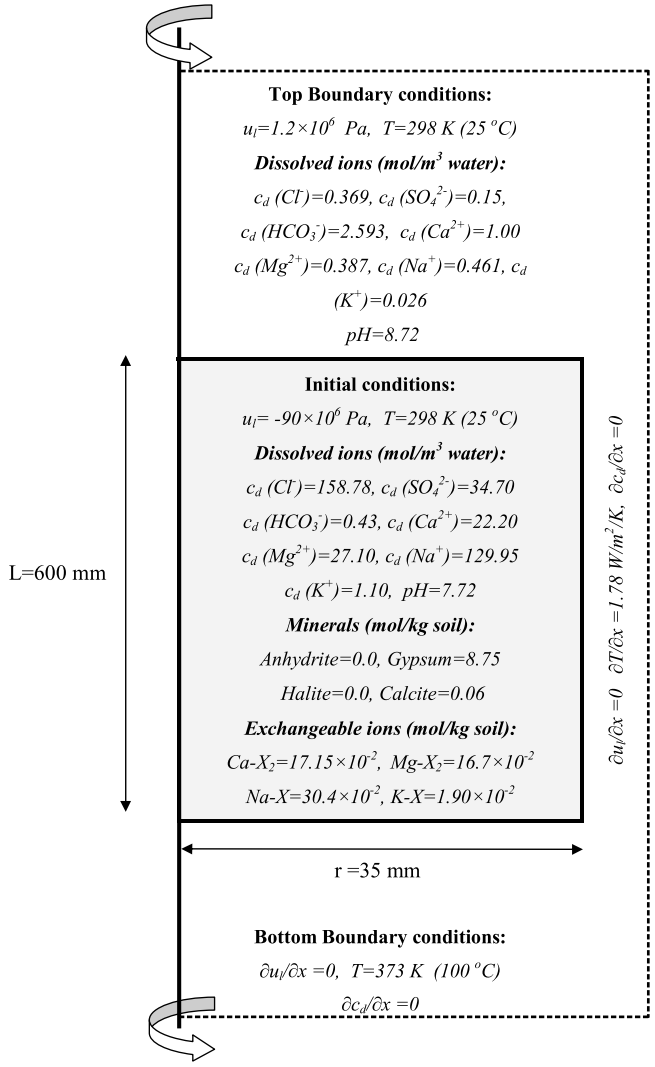

Fig. 2. Initial and boundary conditions applied for coupled thermal, hydraulic, and chemical simulation of the heating and hydration experiments.

Table 1. Thermodynamic parameters used for dissolution/precipitation of minerals and the equilibrium constants of the ion exchange reactions for the FEBEX bentonite

Reactions	Thermodynamic parameters: log K_{eq} (25°C)	Thermodynamic parameters: ΔH_r^0 (kcal)
Mineral dissolution/precipitation[a]		
$CaSO_4 = Ca^{2+} + SO_4^{2-}$ (Anhydrite)	−4.360	−1.710
$CaSO_4 \cdot 2H_2O = Ca^{2+} + SO_4^{2-} + 2H_2O$ (Gypsum)	−4.580	−0.109
$NaCl = Na^+ + Cl^-$ (Halite)	1.582	0.918
$CaCO_3 = Ca^{2+} + CO_3^{2-}$ (Carbonate)	−8.480	−2.297
Ion exchange[b]		
$Na\text{-}X = Na^+ + X^-$	0.0	—
$Ca\text{-}X_2 = Ca^{2+} + 2X^-$	0.774	—
$Mg\text{-}X_2 = Mg^{2+} + 2X^-$	0.655	—
$K\text{-}X = K^+ + X^-$	0.878	—

[a]Data from the phreeqc.dat database by Parkhurst and Appelo (1999).
[b]Data from Fernández et al. (2001).

Table 2. Initial geochemistry of the clay-water system and injected aqueous solution

Pore fluid chemistry	Initial pore water	Inflow water	Unit
	Dissolved ions		
Cl^-	158.8	0.369	mol/m^3
SO_4^{2-}	34.7	0.150	mol/m^3
HCO_3^-	0.43	2.593	mol/m^3
Ca^{2+}	22.2	1.00	mol/m^3
Mg^{2+}	27.1	0.387	mol/m^3
Na^+	129.9	0.461	mol/m^3
K^+	1.10	0.026	mol/m^3
pH	7.72	8.72	—
	Mineral contents		
Anhydrite	0	—	mol/kg soil
Gypsum	0.0054	—	mol/kg soil
Halite	0	—	mol/kg soil
Calcite	0.06	—	mol/kg soil
	Exchangeable contents		
Ca-X_2	17.1×10^{-2}	—	mol/kg soil
Mg-X_2	16.7×10^{-2}	—	mol/kg soil
Na-X	30.4×10^{-2}	—	mol/kg soil
K-X	1.9×10^{-2}	—	mol/kg soil

pore fluid, and a set of geochemical variables in the domain including minerals, exchangeable ions, and pH. (Referred as the transient analysis). Fig. 3 shows the thermal, hydraulic, and chemical initial and boundary conditions applied that were adopted based on the conditions of the experiments. Constant temperature and water pressure at the top of the domain equal to 298 K and 1.2 MPa, respectively, was considered. A fixed temperature equal to 373 K and impermeable boundary condition to water flow was applied at the bottom of the domain. The boundary conditions for the chemical components at the top of the domain were considered to be fixed concentration whilst at the bottom of the domain, an impermeable

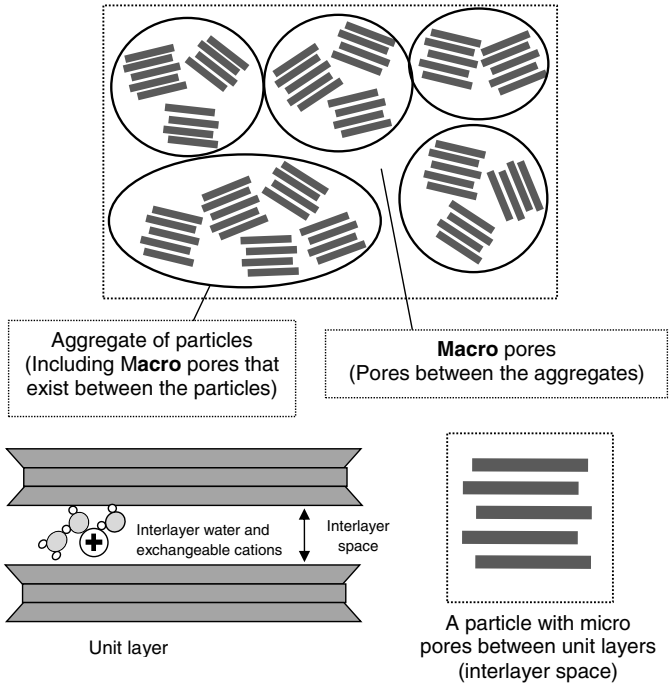

Fig. 3. "Microporosity" and "macroporosity" definition in compacted smectite clay.

boundary was considered. At the radial boundary, a heat flux was applied, representing the potential heat loss from the cell. The heat loss can theoretically be calculated that is equal to 2.3 $W/m^2/K$. This value is obtained by considering a 15 mm PTFE casing having thermal conductivity of 0.25- and 15-mm foam insulation with thermal conductivity of 0.4 W/m/K (Villar et al. 2008b). A lower value of heat flux, i.e., 1.78 $W/m^2/K$, was used in the simulation compared with the value of heat flux which was calculated theoretically, due to the effects of a potential layer of air trapped in the radial boundary of the sample that may have provided an extra isolation layer. The radial boundary is considered to be impermeable to fluid. Precipitation/dissolution of calcite has been considered as a kinetically controlled reaction in the transient analysis, while mineral reactions have been considered as equilibrium reaction for other minerals involved. The kinetic rate of calcite reaction was adopted from the equation and parameters presented in the phreeqc.dat data base of PHREEQC.

The water content and temperature applied during the experimental postmortem geochemical analysis were 400% gravimetric water content (i.e., the ratio of liquid/solid was 4:1) and 25 °C, respectively (Fernández and Villar 2010). These values can be different from the water content and temperature at the corresponding locations in the sample after the completion of experimental tests or transient analysis (0.5, 1.0, 2.0, and 7.6 years). Changes in the water content and temperature during postmortem tests will affect the geochemical equilibrium of the soil-chemical-water system; hence, the composition of ions resulting from the transient analysis at the end of the tests should be reanalyzed to replicate the experimental conditions (water content and temperature) in which the postmortem experiments were carried out. This step of analysis (postmortem analysis) will enable the comparison of transient analysis with postmortem experiments, i.e., provide a validation. The results of numerical simulations including temperature, water content, and geochemical variables obtained from the transient analysis at 0.5, 1.0, 2.0, and 7.6 years were used as initial inputs for calculating the pore water composition of the samples using PHREEQC under the water content and temperature of postmortem experimental conditions of the experiments (i.e., 25°C and 400% gravimetric water content).

In summary, the experimental data used to develop the simulations and comparison with the results of analysis include (1) transient temperature profile and (2) water contents profile and pore fluid chemistry based on the geochemical postmortem analysis at the end of the tests reported.

Material Properties

Thermal and Hydraulic Behavior

The material constants including density of water, density of solid, specific heat capacity of solid, liquid, and vapor, latent heat of vaporization, Henry's constant, and specific gas constant for gas vapor were obtained from the literature (Mayhew and Rogers 1976; ENRESA 2000). Thermal conductivity is calculated by ENRESA (2000):

$$\lambda_T = A_2 + (A_1 - A_2)\left[1 + \exp\left(\frac{S_l - x_0}{d_x}\right)\right]^{-1} \quad (8)$$

where S_l is the degree of saturation, $A_1 = 0.52$, $A_2 = 1.28$, $x_0 = 0.65$, and $d_x = 0.1$.

The moisture retention relationship used is based on the van Genuchten's relationship (van Genuchten 1980) and the parameters provided for compacted FEBEX bentonite by ENRESA (2000):

$$S_l = S_{l0} + (S_{l\max} - S_{l0})\left[1 + \left(\frac{s}{p_0}\right)^{1/(1-\alpha)}\right]^{-\alpha} \quad (9)$$

where s is suction (MPa), $S_{l0} = 0.1$, $S_{l\max} = 1.0$, $p_0 = 30$ MPa, and $\alpha = 0.32$.

Using the moisture retention relationship provided, the initial degree of saturation (58.6%) corresponds to a suction value equal to 90.0 MPa.

As discussed in the introduction section, studies of the hydraulic behavior of compacted bentonite have indicated that the expansion/shrinkage of the clay microstructure during hydration/dehydration show profound effects and control on the moisture flow in compacted bentonite (e.g., Thomas et al. 2003; Sánchez et al. 2012). As shown in Fig. 3, the porosity system of compacted bentonite can be conceptualized at least by two scales of porosity (Sedighi and Thomas 2014): (1) "microporosity" that comprises the pore spaces between the unit layers of smectite or lamellas, (also called interlayer porosity) and (2) "macroporosity" that includes pores between the particles (interparticle pores) and between the aggregates of particles (interaggregate pores). "Microporosity" is always fully saturated and hydration and dehydration processes, therefore, changes the interlayer distance between the clay platelets by adding/removing water molecules. The interlayer hydration and dehydration of smectite involves adsorption or desorption of one to three discrete layers of water molecules between the clay platelets (Pusch and Yong 2006). The crystalline structure of the mineral remains unchanged during the hydration/dehydration process (Ransom and Helgeson 1994). The water molecules within the interlayer space of smectite (micropores), combined with a small portion of water attached to the particle external surfaces, constitutes a proportion of water that is considered to be immobile compared with that located in macropores (Pusch et al. 1990; Hueckel 1992). The pathways for water flow and transport of ionic species in compacted bentonite are practically reduced to the spaces/pores between the particle and aggregates. The macroporosity is (in contrast to the microporosity) a two-phase system that can contain both liquid and vapor. Water molecules can be exchanged between these two scales of porosity.

Thomas et al. (2003), Sedighi (2011), and Thomas and Sedighi (2012) have introduced a form of modified hydraulic conductivity that includes the effects of microstructure swelling on hydraulic conductivity. The concept is based on the assumption that the porosity available to water flow is limited to the macropore spaces between the clay particles and the water that exists in the interlayer porosity is practically immobile. A general form of the modified relationship for the hydraulic conductivity of compacted bentonite is given as follows (Sedighi 2011):

$$k_l = \left(1 - \frac{\theta_{il}}{\theta_l}\right) k_{sat} S_l^{\beta} \quad (10)$$

where k_{sat} is the saturated hydraulic conductivity ($k_{sat} = 3.5 \times 10^{-14}$ m/s for compacted FEBEX bentonite), β is a constant which has been given as 3 for the studied clay (Villar et al. 2008a), and θ_{il} is the volumetric water content of microstructure (interlayer volumetric water content).

The formulation of moisture flow (mass balance) has been applied to the total water content (sum of the moisture content in micropore and macropore). We do not consider a separate mass balance equation for the micropore water evolution as (1) we consider water in the interlayer to be immobile; and (2) we consider the system under equilibrium (i.e., mass exchange between the micro and macro is instantaneous). The effect of microporosity evolution is manifested in the water flux by the hydraulic conductivity relationship that includes, implicitly, the effects of microstructure. It is noted that a double porosity approach with an exchange term that considers a kinetically controlled exchange of water between micro and macro pores would provide a more comprehensive approach. However, this was beyond the scope of the current study.

Comparisons between the experimental results and simulations that consider the modified hydraulic conductivity in hydraulic flow formulations show a closer correlation with the behavior observed in experimental studies of both isothermal and non-isothermal water infiltration (Sedighi 2011; Thomas and Sedighi 2012). Section "Microstructure Evolution during Hydration and Dehydration" describes the approach developed to calculate the interlayer water content.

Microstructure Evolution during Hydration and Dehydration

Compaction of bentonite primarily reduces the macroporosity (Likos and Lu 2006). Therefore, by increasing the dry density of compacted bentonite, it is expected that the contribution of interlayer porosity to the overall porosity increases. During hydration of smectite, a number of discrete layers of water are entered into the variable pore space between the individual unit layers of smectite (interlayer porosity). A maximum number of 3–4 layers of water molecules can be adsorbed in the smectite interlayer that correspond to the basal spacing of approximately 1.70–2.0 nm, respectively (Laird 2006). Models for prediction of the interlayer/microporosity variation in compacted bentonite are very limited (especially under variable suction or temperature). The existing prediction are based on the variation of basal spacing between the interlayer platelets, observed in the XRD analysis by which the porosity associated can be calculated by considering a homogeneous distribution of parallel clay platelet in the system (Likos and Lu 2006; Warr and Berger 2007; Likos and Wayllace 2010; Holmboe et al. 2012).

Sedighi and Thomas (2014) have proposed a generic approach to calculate the interlayer porosity/interlayer water content of compacted bentonite and its evolution with environmental conditions (relative humidity and temperature) based on a geochemical model of hydration/dehydration of smectite proposed by Ransom and Helgeson (1994). The interlayer hydration and dehydration of smectite can be described as a geochemical reaction between water molecules and a symbolic hydrous and its homologous anhydrous counterparts of smectite (Ransom and Helgeson 1994; Vidal and Dubacq 2009), described as:

$$Hydrous\ smectite\ (hs) \leftrightarrows Anhydrous\ smectite (as) + n_m H_2O$$

where, n_m is the number of moles of water present in the interlayer adsorption or desorption reaction, given as the moles of water per smectite half formula unit, i.e., $O_{10}(OH)_2$ (Ransom and Helgeson 1994).

Ransom and Helgeson (1994) have shown that solid solution reaction of interlayer hydration/dehydration can be expanded as (Ransom and Helgeson 1994):

$$\log K_{eq} = \log\left(\frac{1 - X_{hs}}{X_{hs}}\right) + \frac{W_s}{2.303RT}(2X_{hs} - 1) + n_m \log a_w \quad (11)$$

where K_{eq} represents the equilibrium constant of the reaction and X_{hs} represents the mole fraction of the hydrous smectite and W_s denotes the Margules parameter for the binary regular solid-solution of hydrous and anhydrous smectite components at reference temperature (25 °C) and pressure (0.1 MPa), which is independent of

pressure and temperature (Ransom and Helgeson 1994). The gas constant is referred to as R and a_w is the activity of water.

Sedighi and Thomas (2014) have presented a calculation of the interlayer porosity/interlayer water content as a function of the mole fraction of hydrous smectite in the interlayer hydration/dehydration reaction of smectite. Accordingly, the interlayer volumetric water content can be given as (Sedighi and Thomas 2014)

$$\theta_{il} = X_{hs} \frac{n_m v_{il}}{m_{sm}} \rho_d^{sm} \tag{12}$$

where v_{il} denotes the specific molar volume of the interlayer water, m_{sm} is the molar mass of dry smectite, and ρ_d^{sm} represents the bulk dry density of smectite.

It is noted that as the interlayer space remains always saturated. Therefore, the porosity associated with the microstructure (n_{il}) is equivalent to the interlayer volumetric water content (θ_{il}).

Based on Eq. (11), the mole fraction of hydrous smectite can be calculated by knowing the equilibrium constant of the reaction ($\log K_{eq}$), the Margules parameter (W_s), and the mole number of hydrate water in a fully hydrated smectite (n_m) at given temperature (T) and water activity (a_{H_2O}). Assuming the molar volume of interlayer water to be same the same as that in macro pore, the activity of water can be expressed in terms of the relative humidity (or total suction) of the macro pore or the surrounding environment.

The thermodynamic parameters of the solid-solution model for pure smectites, including the equilibrium constants of the reactions and the Margules parameters were reported by Ransom and Helgeson (1994). The parameters have been derived based on calibration of the model against laboratory-based vapor adsorption data of powdered smectite samples. The equilibrium constant of the reaction ($\log K_{eq}$) varies with temperature (Ransom and Helgeson 1995), which is calculated as a function of the standard enthalpy of reaction ($\Delta H^0_{r,T_r}$) at reference temperature (T_r) and the standard heat capacity of the reaction at constant pressure, (ΔC_p^0) given as (Langmuir 1997)

$$\log K_{eq} = (\log K_{eq})_{T_r} + \frac{\Delta H^0_{r,T_r}}{2.303R}\left(\frac{1}{T_r} - \frac{1}{T}\right) + \frac{\Delta C_p^0}{2.303R}\left(\frac{T}{T_r} - 1\right) + \frac{\Delta C_p^0}{2.303R}\ln\left(\frac{T}{T_r}\right) \tag{13}$$

In this study we adopted the thermodynamic parameters for the hydration/dehydration reactions for homo-ionic smectite presented by Ransom and Helgeson (1994) considering FEBEX bentonite as a mixture of Ca, Mg, and Na smectite. Table 3 presents a summary of the parameters used to calculate the microporosity variation.

Chemical Transport Behavior

Two series of parameters required for modelling the reactive transport of chemicals include (1) transport properties and (2) thermodynamic and kinetic parameters of the geochemical reactions. The geochemical reaction parameters have been described in Table 1. The transport parameters required are those related to the molecular diffusion and thermal diffusion processes in according to Eqs. (5)–(7).

García-Gutiérrez et al. (2004) studied the diffusion properties of FEBEX bentonite and have shown that the accessible porosity for HTO agrees well with the total porosity, which implies that all the pores in compacted bentonite are available for diffusion of neutral species. The accessible porosity for the diffusion of chloride tracer was reported to be considerably smaller than the total porosity, even at the lower densities, demonstrating a significant anionic exclusion. Their results indicated that the accessible porosity for chloride is a small fraction of total porosity (2–3%) at a dry density of 1,650 kg/m^3. The tortuosity factors for anionic and cationic species (τ_i) were therefore considered to be different in this study. The effects of tortuous path and constrictivity (together) were included by considering different effective porosities for diffusion of anionic and cationic species. A modified form of the tortuosity factor proposed by Revil and Jougnot (2008) was used in which the porosity is replaced by the effective porosity. The relationship used to describe the tortuosity factor is

$$\tau_i = (n^i_{eff})^{\beta-1}(S_l - S^c_l)^{\gamma-1} \tag{14}$$

where n^i_{eff} is the effective porosity for diffusion of the i^{th} ionic species, S^c_l is the percolation threshold for degree of saturation, suggested by Revil and Jougnot (2008), and β and γ are constants. In this study the values of S^c_l, β, and γ were considered to be 0, 2.5, and 2.75, respectively.

The effective porosity for the anionic diffusion is described by

$$n^{Anions}_{eff} = n - n_{il} - n_{DDL} \tag{15}$$

where n_{il} represents the interlayer porosity calculated from the hydration/dehydration model [based on Eq. (12)] and n_{DDL} is the porosity associated with the developed diffusion layer.

The effective porosity for chloride diffusion has been given in the range of 0.02–0.03 for fully saturated FEBEX bentonite, compacted at dry density of 1,650 kg/m^3 (García-Gutiérrez et al. 2004). Applying Eq. (11) under saturated state and ambient temperature yields the interlayer porosity to be approximately 0.27. The porosity associated with the developed diffusion layer was calibrated as a constant value of 0.105 for the anionic species to produce the effective porosity in the range of 0.02–0.03 at saturated state based on effective porosity values provided by García-Gutiérrez et al. (2004)

Table 3. Parameters used in the hydration/dehydration model for the FEBEX bentonite in order to calculate the interlayer hydrate water content

Parameter	Unit	Ca-smectite	Mg-smectite	Na-smectite
n_c	moles/$O_{10}(OH)_2$		4.5	
v_{il}	m^3/mole		17.22	
m_{sm}	g/mol $O_{10}(OH)_2$		376.234	
ρ_d^{sm}	kg/m^3		1,580	
Composition/thermodynamic				
Content	%	37	34	29
W_s	kcal/mol	−2,883	−2,806	−3,254
$(\log K_{eq})_{T_r}$	$T_r = 25^oC$	−3.61	−4.28	−0.767
$(\Delta H^0_r)_{T_r}$	kcal/mol	9,630	10,609	5,810
ΔC_p^0	cal/mol		69.13	

(i.e., $n_{eff}^{Anions} = 0.4 - 0.27 - 0.105 = 0.025$). Including the above tortuosity factor and volumetric water content using Eq. (11), the corresponding value for the effective diffusion coefficient for chloride in fully saturated FEBEX bentonite compacted at dry density of 1,650 kg/m^3 is obtained equal to 1.27×10^{-12} m^2/s which is close to the experimentally measured value of 1.1×10^{-12} m^2/s (García-Gutiérrez et al. 2004). For all anionic species the same tortuosity factor was applied. The effective porosity of cations was assumed to be the effective porosity for water tracer (HTO) diffusion, given as the total porosity in compacted bentonite soils (García-Gutiérrez et al. 2004). The rate of diffusion rate of cations in compacted bentonite has been reported to be larger than that of HTO and this has been explained to be related to the interlayer diffusion or surface diffusion. In is noted that, in the modelling study presented here, enhanced diffusion rate of cations through potential mechanism such as interlayer or surface diffusion has not been considered. By applying the total porosity to the tortuosity factor presented in Eq. (17), the effective diffusion coefficient for cations is obtained in the range of 6.32×10^{-11} to 1.56×10^{-10} m^2/s. These values are also in agreement with the values reported for HTO effective diffusion coefficient equal to 5.8×10^{-11} m^2/s, for fully saturated compacted FEBEX bentonite at dry density of 1,650 kg/m^3 (García-Gutiérrez et al. 2004).

Thermal diffusion of multicomponent chemicals is considered in accordance to the formulation provided in Eq. (5). The term heat capacity in Eq. (7) is calculated using the theoretical approach proposed by Agar et al. (1989) as

$$Q_i^* = Az_i^2 D_i^0 \tag{16}$$

where A is a constant value that depends on the hydrodynamic boundary condition (i.e., 2.48×10^{12} and 2.20×10^{12} for two different hydrodynamic boundary conditions). An average value of the two hydrodynamic boundary conditions was used for this parameter. Details can be found in Sedighi et al. (2011) and Thomas et al. (2012).

The self-diffusion coefficients of the ionic species in water at 25 °C (D_i^0) were taken from the values reported by Lasaga (1998). The Stokes-Einstein relationship has been used to obtain the self-diffusion coefficient of ions in water at variable temperature (Cussler 1997).

Chloride ion is the dependent component considered in the transport model in relation to the overall charge conservation requirement as explained in Appendix I. In other words, the chemical transport formulation is solved for all chemical components except Cl^-. The concentration of chloride is then calculated from the "no net charge" condition $\sum_{i=1}^{n_c}[\partial(\theta_l z_i c_i \delta V)/\partial t] = 0$ (Appendix I). The charge-balance condition in the geochemical reaction ($\sum_{i=1}^{n_c}[\partial(\theta_l z_i s_i \delta V)/\partial t] = 0$) is also separately satisfied during reaction modelling by PHREEQC by adjusting the pH (i.e., The charge-balance equation is used to calculate pH in batch reactions by PHREEQC).

Results and Discussion

The results of numerical simulations of heat transfer, moisture flow, and reactive transport of chemicals are presented in this section. In terms of temperature evolution in the domain, the results of the transient analysis are compared with the transient results of temperature monitoring from the experiment. The variations of water content are compared with those reported from the postmortem analysis by Villar et al. (2008b). In terms of chemical behavior, the results of two series of analysis are presented: (1) the results of transient analysis from coupled numerical simulations that demonstrate the possible state of soil-water-chemical system at the end of 0.5, 1, 2, and 7.6 years experimental tests; and (2) the results of postmortem analysis that are used to compare against data from the postmortem geochemical experiments provided by Fernández and Villar (2010).

Thermal and Hydraulic Behavior

Fig. 4 presents the results of temperature evolution in the domain and those reported by Villar et al. (2008b). Thermal processes reach relatively quickly the steady state and temperature distribution in the domain remains under stable condition for the periods of analysis. The numerical results agree well with the experimental results. Variations of the degree of saturation are presented in Fig. 5. The experimental profiles of moisture content and dry density in the domain reported by Villar et al. (2008b) were used to compare the variations of the degree of saturation in the domain. It is noted that the porosity was considered to be constant (0.4) to calculate the degree of saturation from water content data reported. From Fig. 5, it can be observed that there is a close agreement between the numerical and experimental results. However, the numerical model has slightly underpredicted the drying at the hot boundary region

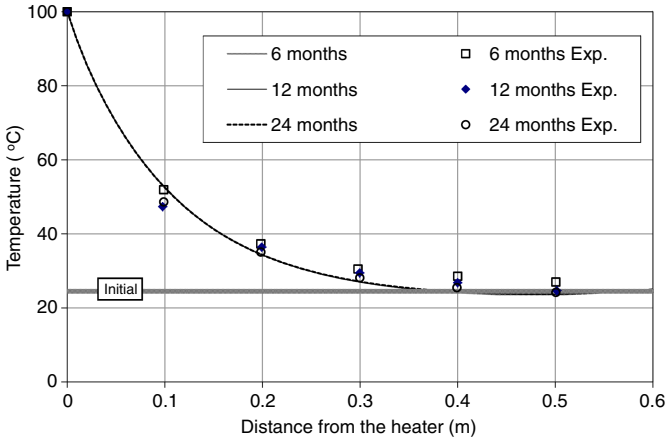

Fig. 4. Variations of temperature in the domain obtained from the transient analysis and experiments. (Experimental data from Villar et al. 2008b.)

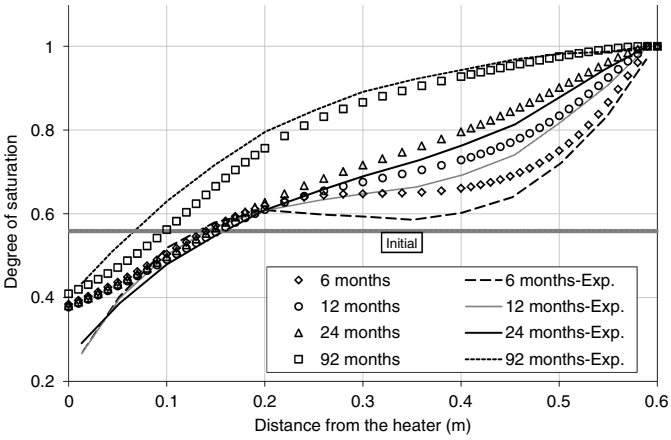

Fig. 5. Variations of degree of saturation in the domain obtained from the transient analysis and experiments. (Experimental data from Villar et al. 2008b.)

for the periods of 6, 12, and 24 months but is well correlated in the case of 92 months. On the hydration side, the model predicted a slightly higher degree of saturation up to 24 months. However, the results are correlated well with the experimental results for the period of 92 months analysis. The parameters used in the vapor transport model, which generally yield higher vapor flux due to the temperature gradient, can be described as reasons behind the higher drying obtained close to the hot boundary. Theoretical understanding of unsaturated bentonite behavior under elevated temperatures is immature due to the degree of complexity and coupling between different processes. The comparison presented highlights the need for further research at lower scales of modelling (i.e., pore scale) that can reduce the level of uncertainty in parameters that are conventionally used in modelling at continuum scale.

The rate of hydration due to the injecting fluid has been gradually reduced and the results correlate with the results of experimental hydration front for the duration of 92 months. This is mainly due to the application of the modified hydraulic conductivity through the interlayer modification factor [i.e., $[1 - (\theta_{il}/\theta_l)]$ in Eq. (10)]. The interlayer hydration process reduces the hydraulic conductivity as the interlayer water ratio approaches higher values. Although the soil deformation was not considered and simulated, the effects of changes in the available porosity for the water flow and transport of chemicals have been considered through the modification of the hydraulic conductivity.

Based on the experimental results (Villar et al. 2008b), the dry density of the samples has changed from an initial value of 1,650 kg/m^3 to a maximum range of 1,700–1,750 kg/m^3 in the vicinity of the heater. On the hydration side, the dray density has reduced to a minimum value of 1,400–1,450 kg/m^3. The total porosity has theoretically be reduced to 0.35 close to the heater and increased to 0.47 in the hydration boundary from its initial value of 0.4. It is therefore anticipated that the overall effects of porosity variation on the flow behavior in the heater zone are limited. Since the overall swelling of the sample was constrained, the increase of porosity in the hydration affected area has reduced the macroporosity that has been captured in the model via the modified hydraulic conductivity relationship used. The deformation effects are likely to be less effective on the overall transport behavior than other processes described. However, it is acknowledged that considering mechanical behavior is required for understanding the swelling pressure development in the system and further accurate description of the mechanically-coupled processes.

Chemical Behavior: Anionic Species

Fig. 6 presents the profiles of chloride (Cl^-) distribution in the domain at different times. Chloride can be considered as a conservative anion; it is not commonly involved in geochemical reactions and not affected by changes in the pH and redox conditions. Therefore, the chloride distribution in the domain has not been affected by the geochemical reactions during the postmortem analysis. The chloride profile related to the transient analysis and postmortem analysis yielded exactly the same values as was expected (Sedighi 2011). The results of postmortem experiments reported by Fernández and Villar (2010) are also shown in Fig. 6. Accumulation of chloride toward heater that is associated with the advective flow of chloride ions, flushed toward the heater from the hydration boundary. The accumulation of the chloride ions in the first 200 mm distance from the hydration side is also observed. The front peak in chloride profile is extended toward the middle of the domain with time. Moreover, due to the increase in temperature in the areas close to the heater, the liquid water moves toward the heater. Chloride ions in the domain have been transferred toward the heater by the liquid

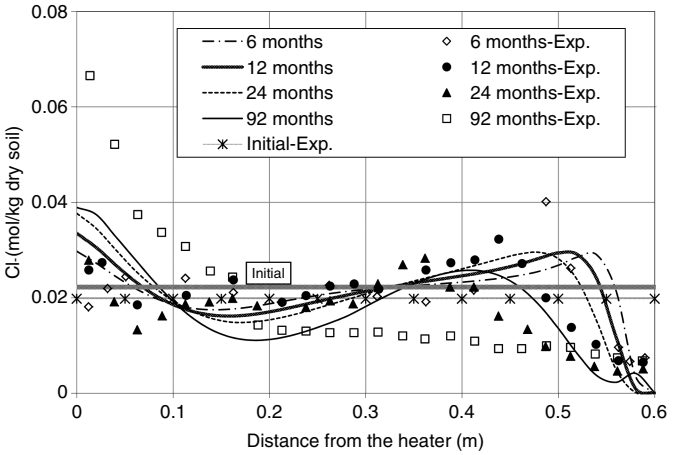

Fig. 6. Variations of chloride in the domain obtained from the transient analysis and experimental results. (Experimental data from Fernández and Villar 2010.)

water flow from the boundary that is an advective dominated process. Moisture transfer can simultaneously take place from the hot end toward the cold region in the form of vapor. Water evaporates while approaching the heater due to the higher temperature and diffuses toward the colder side until it condensates at further distance from the heater. Consequentially, as the pores close to the heater are less saturated, suctions are established. Water then moves toward the heater via advective liquid flow due to the suction gradient. At any location, thermodynamic equilibrium between liquid water and vapor should be achieved at a certain temperature of the studied point in the domain. The chloride ions carried by the liquid flow remained at the hot end, as the moisture content reduces due to the vapor flow induced by elevated temperature. The process of simultaneous water and vapor movement in the areas close to the heater is anticipated to be responsible for the excess accumulation of chloride close to the heater while the chloride content was reduced from the initial amount in the area of approximately 80–300 mm away from the heater.

The magnitudes of the accumulation peaks of chloride in the area of the hydration side are also close to the experimental results for the periods of 6, 12, and 24 months. The results for the first three periods of analysis indicate a similar pattern for the chloride distribution in the vicinity of the heater and in the distance of 100–200 mm away from the heater, respectively. However, the results of the model for the 92 months analysis show a higher amount of chloride in the area of 100–300 mm in the vicinity of the hydration side compared with the experimental results. The model predicted smaller quantities of chloride close to the heater. The experimental results show that chloride was almost removed from the more hydrated 400 mm of bentonite, whereas its concentration showed a sharp gradient in the 200 cm closest to the heater. This observation suggests that there can be further processes involved in controlling the hydraulic conductivity evolution which are not fully captured by the hydraulic conductivity model adopted. This includes thermally coupled processes such as thermal osmosis (e.g., Zagorščak et al. 2017).

Fig. 7 presents the distribution profiles of sulfate ($SO4^{2-}$) in the domain obtained from the transient numerical analysis and postmortem analysis. The distribution of the dissolved sulfate in the case study is controlled by (1) the flow processes associated with thermal and hydraulic variations and (2) mineral reactions involving gypsum and anhydrite. The domain initially contained some gypsum but no anhydrite. The concentration of sulfate has reduced

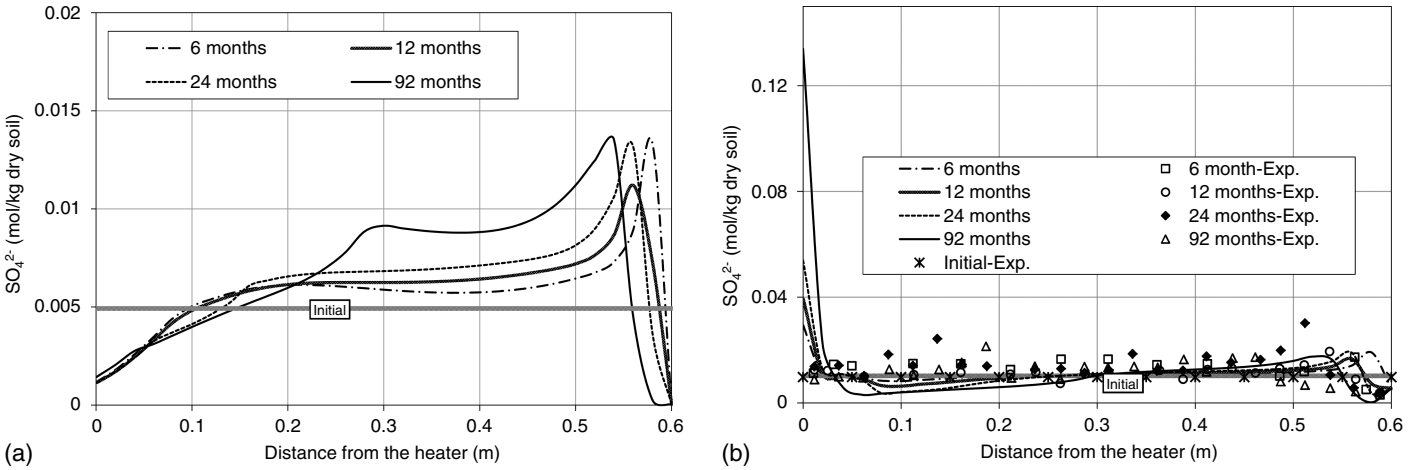

Fig. 7. Variations of sulfate in the domain obtained from the (a) transient analysis; and (b) postmortem analysis (experimental data from Fernández and Villar 2010).

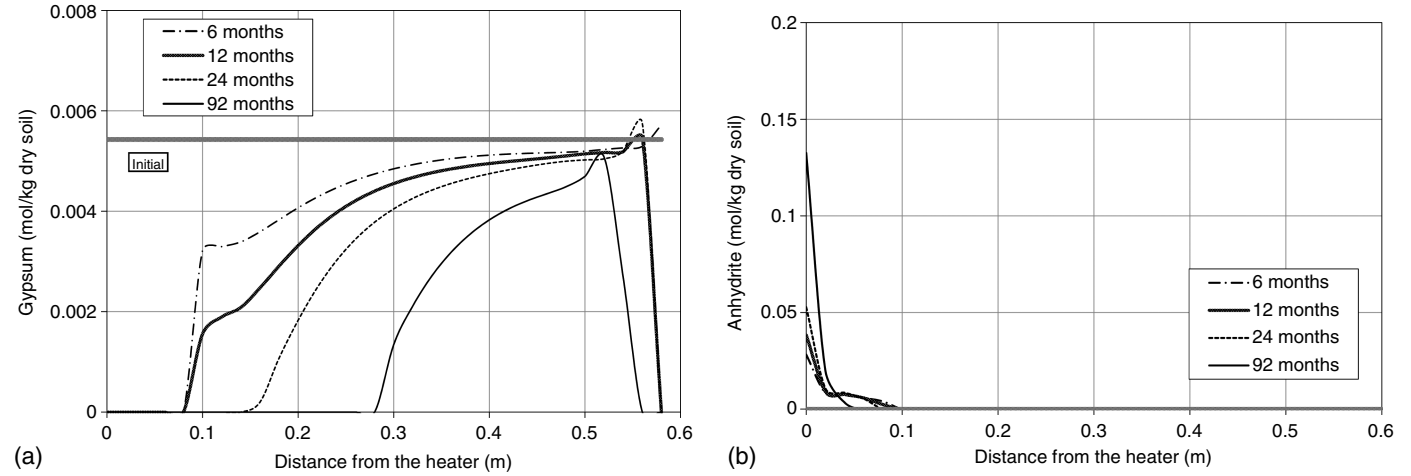

Fig. 8. Variations of (a) gypsum; and (b) anhydrite in the domain obtained from the transient analysis.

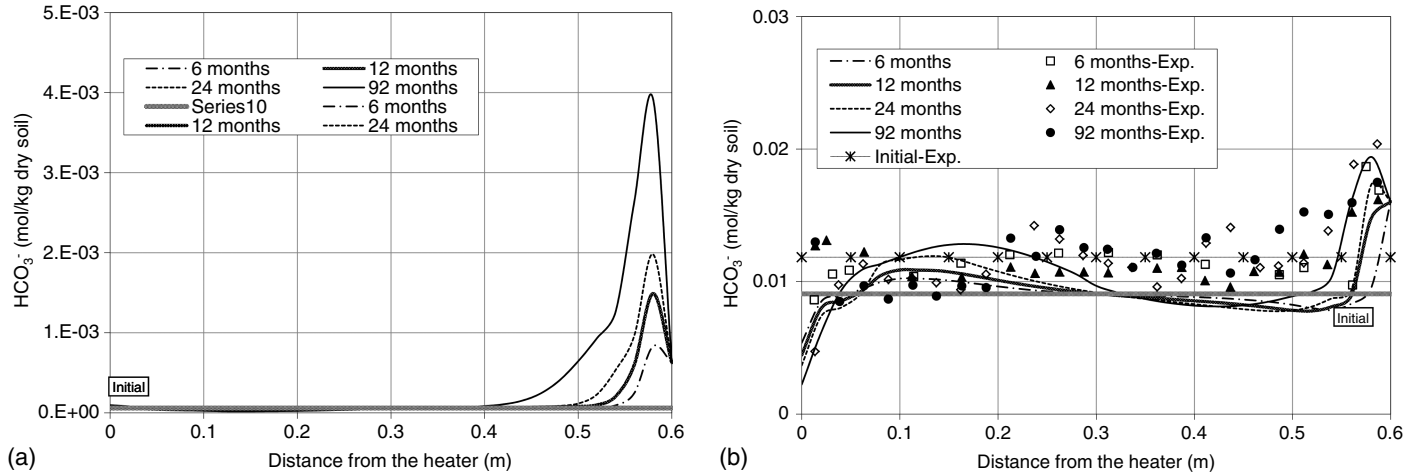

Fig. 9. Variations of bicarbonate in the domain obtained from the (a) transient analysis; and (b) postmortem analysis (experimental data from Fernández and Villar 2010).

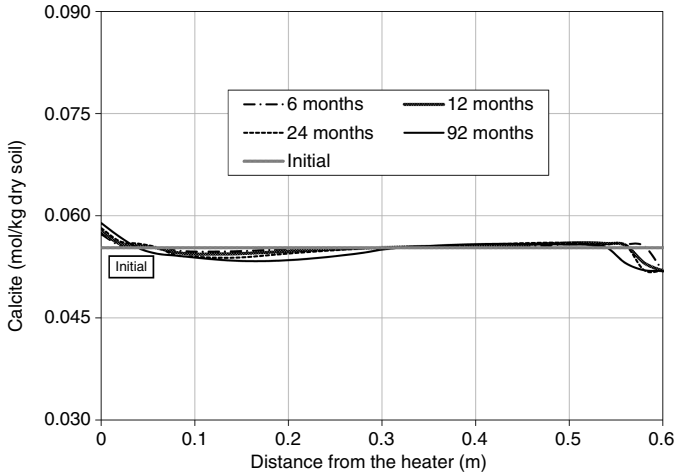

Fig. 10. Variations of calcite in the domain obtained from the transient analysis.

by advancing the hydration front and gypsum has been dissolved that is controlled by the amount of sulphate ions. The results of gypsum distribution in the domain, presented in Fig. 8, indicate that almost all gypsum was dissolved in 50 mm distance from the hydration boundary. The peak of leached sulfate in the hydration side is also located in the same region where gypsum has been dissolved. High and constant concentration of sulfate is observed for the distance of approximately 250 mm distance between 50 mm to 300 mm away from the hydration end, which is due to the gypsum dissolution according to the results presented in Fig. 5. The amount of sulfate shows a decrease in the areas close to the heater. This is believed to be related to the precipitation of anhydrite as it can be seen in Fig. 8. The equilibrium constant of mineral reactions for gypsum and anhydrite are very close while their enthalpies of reaction are different, leading to a different behavior of these two minerals at the regions of higher temperature. The distribution of the dissolved sulfate close to the heater is attributed to the precipitation of anhydrite due to the higher temperature in the domain. Based on the results presented in Fig. 8, a considerable amount of anhydrite has been precipitated in the vicinity of the heater.

Fig. 7 presents a comparison between the results of postmortem analysis and experiments for the dissolved sulfate in the domain. There is a qualitative agreement in terms of the distribution pattern between the model and experimental results. In the area of hydration, the numerical model predicted the sulfate contents close to the experimental results. However, the locations of peaks are slightly different in the model compared with the experimental results. The model shows an overprediction at the hot end and an underprediction in the area close to the hot end, affected by the coupled thermally induced liquid-vapor movement. It is anticipated that the

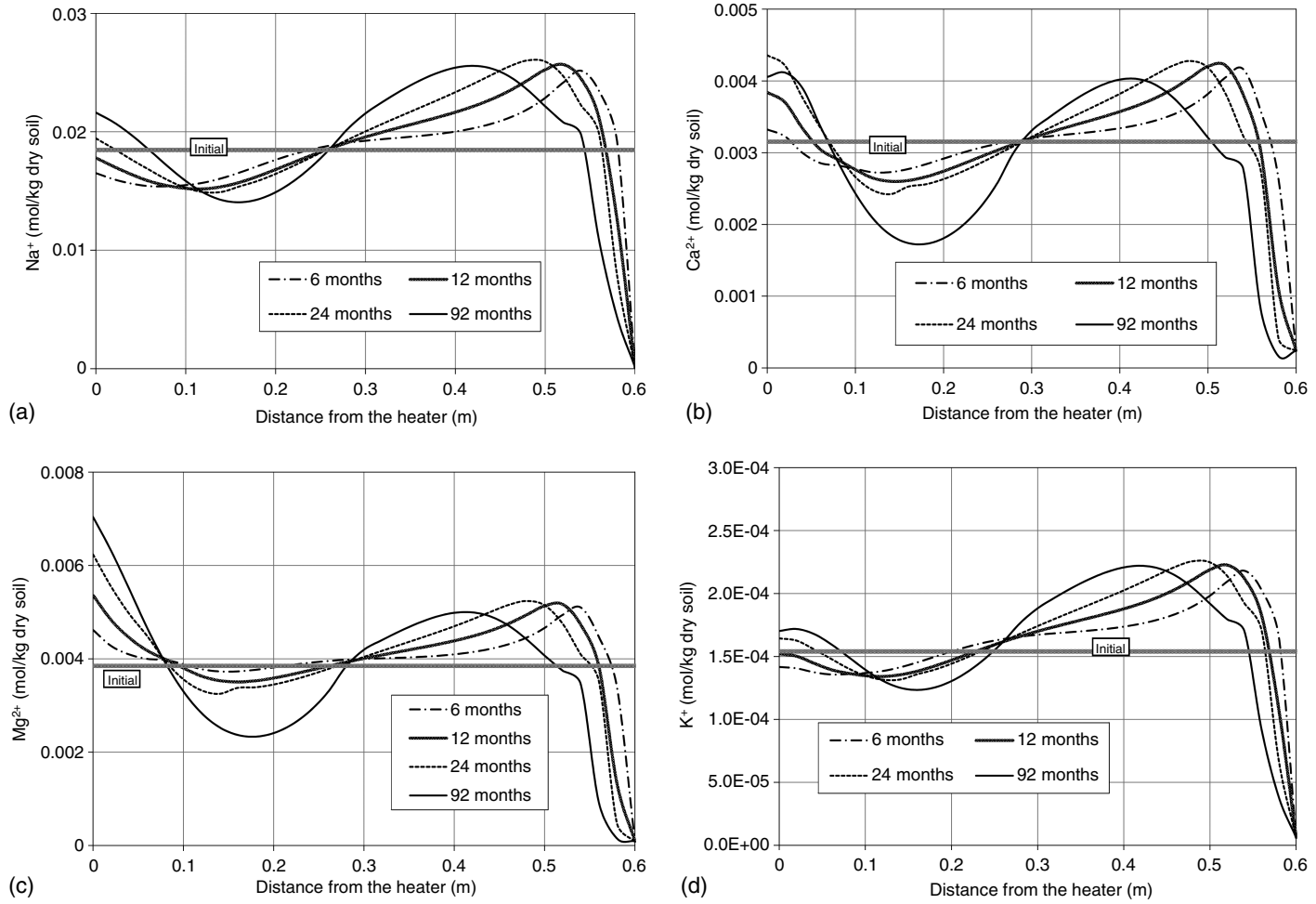

Fig. 11. Variations of (a) sodium; (b) calcium; (c) magnesium; and (d) potassium ions in the domain obtained from transient analysis.

J. Geotech. Geoenviron. Eng., 2018, 144(10): 04018075

overprediction at the hot end is due to the high amount of anhydrite precipitation in the transient numerical modelling results.

Fig. 9 shows the results of transient simulation and postmortem analysis for the dissolved bicarbonate (HCO_3^-). Bicarbonate ions have been transferred to the domain by the water at the hydration boundary, which has resulted in accumulation of bicarbonate in a limited region close to the boundary. As shown in Fig. 10, the overall amount of calcite has not significantly changed for different periods of analysis compared to the initial value. This is due to the low rate of precipitation/dissolution of calcite. Localized precipitation of calcite has occurred in the vicinity of the heater as results of lower initial concentrations of bicarbonate and higher initial concentration of calcium. The results of XRD analysis (Villar et al. 2008b) show a slight decrease in the calcite content in the 92 months test. A comparison between the postmortem analysis results against the experimental results for the dissolved bicarbonate concentration is presented in Fig. 9. A close agreement in terms of distribution pattern for all time intervals can be highlighted. The concentration of bicarbonate shows an increase in the hydration side that is consistent with experimental observations. This is anticipated to be attributed to the localized dissolution of calcite in the hydration end (Fig. 7). The results indicate that the calcite dissolution has occurred in a region of about 100 mm close to the hydration side. In this region, a lower amount of calcium and high amount of bicarbonate existed prior to the postmortem analyses. As a result, calcite is dissolved to maintain the equilibrium condition. The reduced bicarbonate content can be correlated to dissolution of calcite at the heating boundary as also noted by Fernández and Villar (2010).

Chemical Behavior: Cationic Species and pH

Fig. 11 present the results of numerical simulation for the dissolved cationic species including sodium (Na^+), calcium (Ca^{2+}), magnesium (Mg^{2+}), and potassium (K^+) in the domain. Similar distribution patterns for the cationic species are observed. The concentrations of cationic species are observed to be reduced in the vicinity of the hydration side due to the advection process. The ions flushed through the sample have been accumulated in the first half of the domain away from the hydration side. Cationic species have been transferred by the advection and diffusion toward the heater, providing areas with greater concentrations than the initial value within a length that ranges between 50 mm to 350 mm away from the hydration source. The increased concentrations of cations close to the heater and their reduction in the areas approximately between 50 and 300 mm away from the heater are controlled by the simultaneous water and vapor flow in the area within the 300 mm distance from the heater.

The transport processes of sodium ions were only affected by the ion exchange reaction as the sodium ions were not involved in any mineral precipitation and dissolution reactions. Fig. 12 presents the variations of exchangeable sodium in the domain obtained from the numerical analysis. Except for limited regions close to the boundaries, small variations from the initial amount of the exchangeable

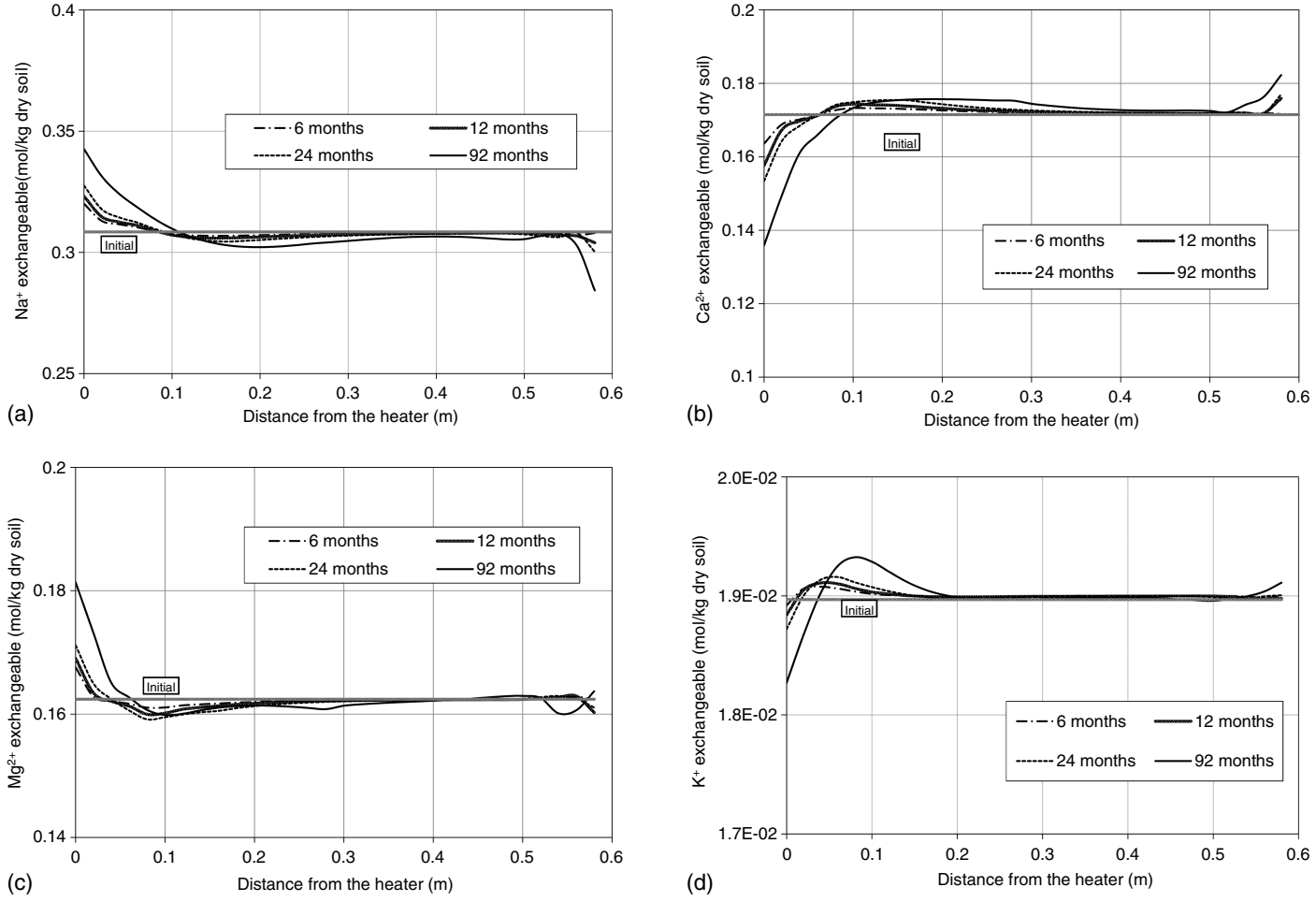

Fig. 12. Variations of (a) sodium, (b) calcium, (c) magnesium, and (d) potassium exchangeable ions in the domain obtained from transient analysis.

J. Geotech. Geoenviron. Eng., 2018, 144(10): 04018075

sodium can be observed. The evolution of the exchangeable sodium is driven mainly by the excess amount of calcium in the vicinity of the heater, which resulted to the replacement of the sodium ions by calcium ions in the interlayer. On the other hand, the calcium concentration was reduced in the solution in the distance of 20–300 mm, providing the conditions for the replacement of calcium by sodium ions in the interlayer. The distribution of the dissolved calcium in the domain was affected by the presence and evolution of the mineral reactions (anhydrite, gypsum, and calcite) and ion exchange reactions. The effects of mineral reaction are mainly related to the dissolution of gypsum and precipitation of anhydrite rather than calcite.

From Fig. 11, it can be observed that the concentration of magnesium decreased by the advection and increased in the first 250 mm away from the injection point. It is noted that only ion exchange has been involved as a chemical reaction that involves magnesium in the numerical analysis. Dissolution/precipitation of dolomite was not considered and that may cause some level of uncertainty about the fate of magnesium. However, it is anticipated that the transport processes had a greater contribution in the evolution of magnesium. As shown in Fig. 12, limited variation of the exchangeable magnesium in the domain has occurred, except in the region affected by the elevated temperature. The pore fluid in this region contained larger amount of sodium and magnesium than that of calcium due to the precipitation of anhydrite. This resulted in the replacement of calcium exchangeable ions with sodium and magnesium.

Fig. 11 also shows the distribution profiles of potassium in the domain. The behavior is more similar to those observed for sodium and magnesium that that of calcium. From Fig. 12, it can be observed that potassium exchangeable ions were replaced by sodium and magnesium ions in the interlayer in the region close to the heater. It is noted that only ion exchange reactions have geochemically affected the distribution of potassium.

The results of postmortem analysis and the experimental data for the dissolved sodium are presented in Fig. 13. The overall trend of distribution is in agreement with the experimental results for all time intervals. In the area close to the heater, a higher concentration of sodium ions is observed from the numerical analysis than those reported from the experiments. This can be explained by the higher drying predicted by the model for the periods of 6, 12, and 24 months at this region. Elevated temperature has controlled the dissolution of anhydrite and precipitation of anhydrite in the vicinity of the heater alongside the transport processes. The behavior of calcium is governed by the combined effects of advection-diffusion of excess ions and geochemical reactions. The distribution of magnesium (Fig. 13) shows a reduced concentration in areas close to the hydration. The concentration of magnesium was increased close to the heater and reduced in the area between about 50–300 mm from the heater, which is qualitatively in agreement with the experimental result. The increase in magnesium content observed in the experimental tests is described to be influenced by temperature (near the heater) and the advance of the water front along the

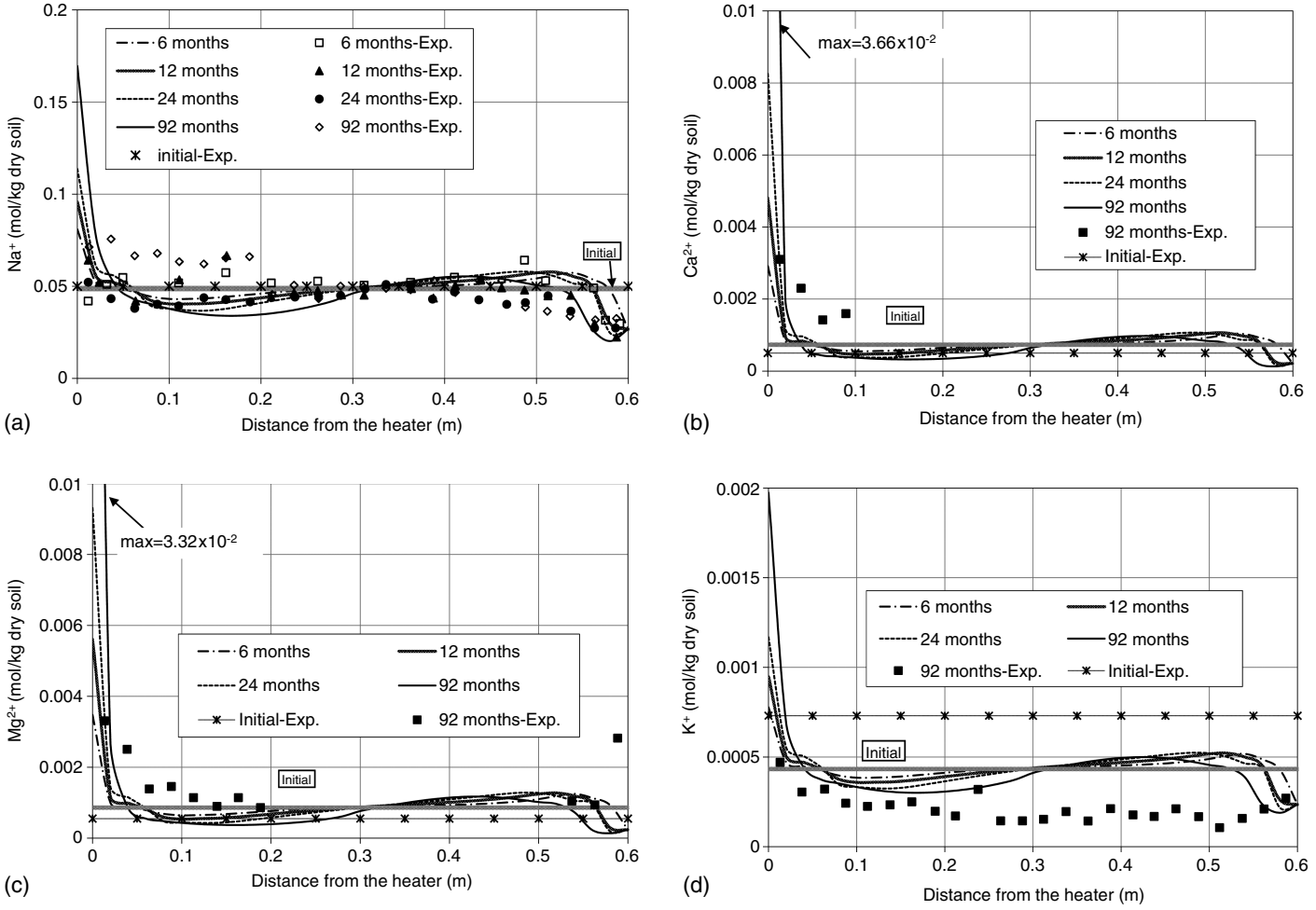

Fig. 13. Variations of (a) sodium; (b) calcium; (c) magnesium; and (d) potassium ions obtained by the postmortem analysis and experiments. (Experimental data from Fernández and Villar 2010.)

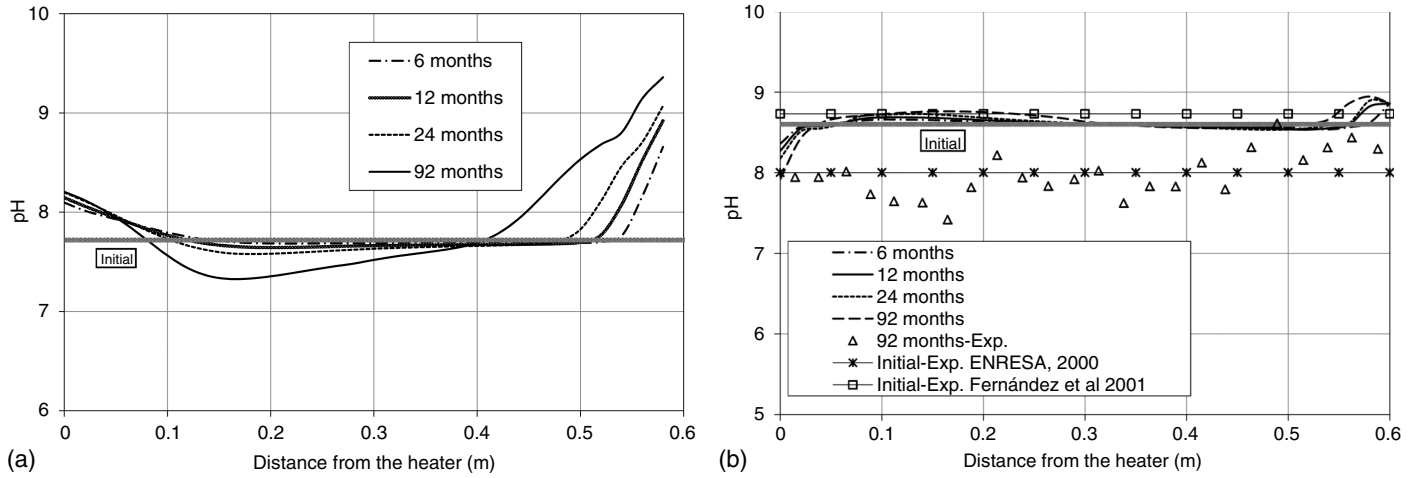

Fig. 14. Variations of pH in the domain obtained from the (a) transient analysis; and (b) postmortem analysis (experimental data from Fernández and Villar 2010).

bentonite column (Fernández and Villar 2010). Fernández and Villar (2010) reported that for all tests, there was an increase in the soluble Mg^{2+}, Na^{+}, K^{+}, and Ca^{2+} concentrations close to the heater, whereas the K^{+} content decreased near the hydration source and Na^{+} decreased in that region. From Fig. 13, it can be observed that the amount of potassium has been reduced in a limited area close to the hydration. The potassium ions transferred by water have been added in the first half of the domain at the hydration side. A high amount of potassium was precipitated due to water-vapor advection process in the 300 mm distance for the heater, which is similar to the behavior of other cations.

As shown in Fig. 12, the exchangeable composition of ions shows higher amount of sodium and magnesium from the initial state close to the heater. The concentration of calcium and potassium ions in the exchangeable composition is reduced due to precipitation of anhydrite and dissolution of gypsum at the hot boundary region. This is also compatible with observation of the pore fluid composition in the region that contains higher concentrations of sodium and magnesium than calcium. Potassium exchangeable ions have also been replaced by sodium and magnesium ions to a lesser extent, providing a new equilibrium condition in the exchangeable composition.

The results of pH variation of the soil water system from the transient numerical simulation are presented in Fig. 14. The variation of H^{+} ions (and pH) is governed only by the geochemical reactions in the transient numerical analysis as H^{+} was not considered in the transport analysis. The pH was calculated in the charge balance of geochemical analysis by PHREEQC (Parkhurst and Appelo 1999). The variation of pH in the domain shows a similar pattern to that presented for the bicarbonate in the hydration zone. As shown in Fig. 9, a high amount of bicarbonate has been accumulated in the hydration affected zone. The pH decreases from the initial value in the domain from 200 mm to approximately 500 mm away from the hydration side and increases over the 92 months of the analysis. The pH decrease in this region can be explained by the dissolution of gypsum and accumulation of sulfate in the soil water. An increase in pH is observed in the vicinity of the heater for up to approximately 100 mm distance from the heating boundary. This is related to the precipitation of anhydrite where the gypsum content was reduced.

Fig. 14 shows the results of postmortem modelling of pH and provides a comparison between the numerical prediction against the experimental results reported by Fernández and Villar (2010). The experimental results reported were only available for the 92 months analysis. The pH evolution shows limited increase in the hydration side and decrease in the area close to the heating boundary. The behavior exhibits similar trend to that observed for bicarbonate. The results are in qualitative agreement with the overall observed in the experiment. The decrease in pH in the heater side can be attributed to the precipitation of calcite. The calcite dissolution has similarly governed the increase in pH in the hydration side. As shown in Fig. 14, the results of postmortem analysis for pH for the 92 months duration are generally higher than those reported by Fernández and Villar (2010). This is related to the difference between the initial pH value used in the numerical simulation and that of the experiment reported by Fernández and Villar (2010). The initial pH used in the numerical analysis (i.e., pH = 8.60) was calculated from the geochemical pore water simulation (Table 2) that is in close agreement with the experimental value reported by Fernández et al. (2004) (i.e., pH = 8.73). It is noted that the pH of FEBEX bentonite reported at the same solid/water ration reported by ENRESA (2000) is lower (i.e., pH = 7.93). The difference can be related to variations of the FEBEX material and its constituents used in ENRESA (2000) and Fernández et al. (2004).

Conclusions

The analysis of coupled thermal, hydraulic, and chemical behavior of compacted bentonite presented here highlights key geochemical reactions involved under the heating and hydration conditions imposed by the compacted bentonite buffer. Using the experimental results of up to 92 months the validity of the theoretical formulations and numerical model developed under the conditions of the problem studied has been examined. The results indicated that temperature variation in the system reached steady-state conditions within a considerably shorter time compared with the hydraulic and chemical processes.

The impacts of the interlayer water on the hydraulic flow behavior were considered via the interlayer hydration model that addresses the major effect of microstructure swelling/shrinkage on flow behavior. The model also showed a close correlation with respect to the saturation period of the FEBEX bentonite by using the proposed unsaturated hydraulic conductivity. Elevated temperature in the heater side showed a profound effect on the distribution of ions and minerals. Higher flow of water and vaporization is likely

to have occurred in the system, facilitating the migration of major ionic species toward the heater by advection mechanism.

The simulation results of the chloride ions showed a good qualitative agreement with the experimental results, especially for the periods of 6, 12, and 24 months. The lower chloride concentration from numerical simulation compared to those reported in the experiment indicates that further processes can be involved that control the flow regime of moisture in the system in the areas affected by the temperature (where the cycle of evaporation-condensation mainly controlled the distribution of chloride). The long term results (92 months) highlight that further development on the hydraulic conductivity model or inclusion of thermally coupled processes is required. The accessory minerals in FEBEX bentonite such as gypsum and carbonates (despite the small proportion in the composition) showed considerable effects on the distribution of anionic species. The fate of cationic species was found to be mainly controlled by the transport processes. The model showed compatible trends in comparison with the pore fluid composition observed with the available experimental dataset. Gypsum was found to be dissolved in the area close to the heating boundary, producing a considerable amount of dissolved sulfate. The composition of exchangeable ions remained the same as the initial condition except mainly for limited distances from the heater based on the transient simulation results. This indicates the possibility of conversion of FEBEX bentonite from Ca/Mg-smectite clay to Na/Mg smectite. The consequences in the long term can affect the swelling pressure predicted for the clay buffer. The research presented provides further insights into the hydro-geochemically coupled process in compacted bentonite buffer and its evolution under the thermal and hydraulic conditions of the geological disposal for high-level radioactive waste.

Appendix I. Formulations of Multicomponent Ionic Transport

The mass conservation equation for the i^{th} chemical component in multi-ionic system of unsaturated porous media can be written in a general form as

$$\frac{\partial(\theta_l c_i \delta V)}{\partial t} + \frac{\partial(\theta_l s_i \delta V)}{\partial t} + \delta V \nabla \cdot J_i = 0 \tag{17}$$

where J_i is the total chemical flux accounting for the sum of advective, diffusive, and dispersive fluxes.

An aqueous solution is electrically neutral on macroscopic scale and the charge should remained balanced (Lasaga 1979). The general form of charge conservation on the transport processes can be given as (Sedighi et al. 2011)

$$\sum_{i=1}^{n_c} \frac{\partial(\theta_l F z_i c_i \delta V)}{\partial t} + \sum_{i=1}^{n_c} \frac{\partial(\theta_l F z_i s_i \delta V)}{\partial t} + \sum_{i=1}^{n_c} \delta V \nabla \cdot F z_i J_i = 0 \tag{18}$$

where F is Faraday constant.

Assuming that the charge is separately conserved in geochemical reactions, (i.e., $\sum_{i=1}^{n_c}[\partial(\theta_l z_i s_i \delta V)/\partial t] = 0$), the electroneutrality for the transport part can be divided into two separate requirements (e.g., Lasaga 1979): (1) the total charge should be conserved (i.e., no net charge $\sum_{i=1}^{n_c}[\partial(\theta_l z_i c_i \delta V)/\partial t] = 0$); and (2) no electrical current should run through the solution (i.e., no current condition $\sum_{i=1}^{n_c} \delta V \nabla \cdot (z_i J_i) = 0$).

Sedighi et al. (2011) and Thomas et al. (2012) have proposed a general formulation for the diffusive flux in aqueous solution due to concentration potential, electrical potential, and thermal potential by expanding the formulations proposed by Lasaga (1979) for multicomponent chemical diffusion and the heat of transport by Ballufi et al. (2005), given as

$$J_i^{diff} = -\frac{D_i^0 c_i}{RT}\frac{\partial \mu_i}{\partial c_i}\nabla c_i - \frac{D_i^0 F z_i c_i}{RT}\nabla \Phi - \frac{D_i^0 c_i Q_i^*}{RT^2}\nabla T \tag{19}$$

where μ_i is the chemical potential of the i^{th} component, Φ is the electrical potential, and Q_i^* represents the heat of transport of the i^{th} component.

The gradient of electrical potential can therefore be determined explicitly by considering "no current condition" $[\sum_{j=1}^{n_c} \delta V \nabla \cdot (z_j J_j) = 0]$:

$$\Delta \Phi = -\frac{1}{F}\left[\frac{\sum_{j=1}^{n_c} D_j^0 z_j c_j \frac{\partial \mu_j}{\partial c_j}\nabla c_j + \sum_{j=1}^{n_c} D_j^0 z_j c_j \frac{Q_j^*}{T}\nabla T}{\sum_{j=1}^{n_c} D_j^0 z_j^2 c_j}\right] \tag{20}$$

The derivative of chemical potential with respect to concentration is (Oelkers 1996)

$$\frac{\partial \mu_j}{\partial c_j} = -\frac{RT}{c_j}\left[1 + \frac{\partial \ln \gamma_i}{\partial c_i}\right] \tag{21}$$

Substituting the electrical potential from Eq. (21) into Eq. (19) yields

$$\begin{aligned} J_i^{diff} = & -D_i^0\left(1 + \frac{\partial \ln \gamma_i}{\partial c_i}\right)\nabla c_i \\ & + \frac{D_i^0 z_i c_i}{\sum_{z=1}^{n_c} D_z^0 z_z^2 c_z}\sum_{j=1}^{n_c} D_j^0 z_j\left(1 + \frac{\partial \ln \gamma_i}{\partial c_i}\right)\nabla c_j - \frac{D_i^0 c_i Q_i^*}{RT^2}\nabla T \\ & + \frac{D_i^0 z_i c_i}{\sum_{z=1}^{n_c} D_z^0 z_z^2 c_z}\sum_{j=1}^{n_c} D_j^0 z_j c_j \frac{Q_j^*}{RT^2}\nabla T \end{aligned} \tag{22}$$

The total flux due to advection, diffusion, and dispersion can be implemented in the mass conservation that yields

$$\begin{aligned} & \frac{\partial(\theta_l c_i \delta V)}{\partial t} + \frac{\partial(\theta_j s_i \delta V)}{\partial t} \\ & = -\delta V \nabla \cdot \left(c_i \mathbf{v}_1 - \sum_{j=1}^{n_c} \theta_l \tau_i D_{ij} \nabla c_j - \theta_l \tau_i D_i^T \nabla T - \mathbf{D}_m \nabla c_j\right) \end{aligned} \tag{23}$$

The overall charge is conserved by implementing the "no charge" and "no current" conditions. In addition, the electroneutrality must be maintained in the geochemical reactions model too. The charge conservation in the reactions is adjusted by the pH in the solution in PHREEQC (Parkhurst and Appelo 1999). The advective and dispersive fluxes are not considered in the "no current" condition (all ions move with the same rate). If the overall charge conservation equation is explicitly employed in combination with the n_c conservation equations for mass, an overdetermined system of equations is obtained (Lasaga 1979; Boudreau et al. 2004). As proposed by Lasaga (1979), one of the concentrations and its derivatives needs to be eliminated from all the equations. A particular dependent ion is therefore eliminated from the model while its concentration is calculated from $(n_c - 1)$ components by the charge conservation equation (Lasaga 1981; Boudreau et al. 2004). In other words, the mass conservation is solved for $(n_c - 1)$

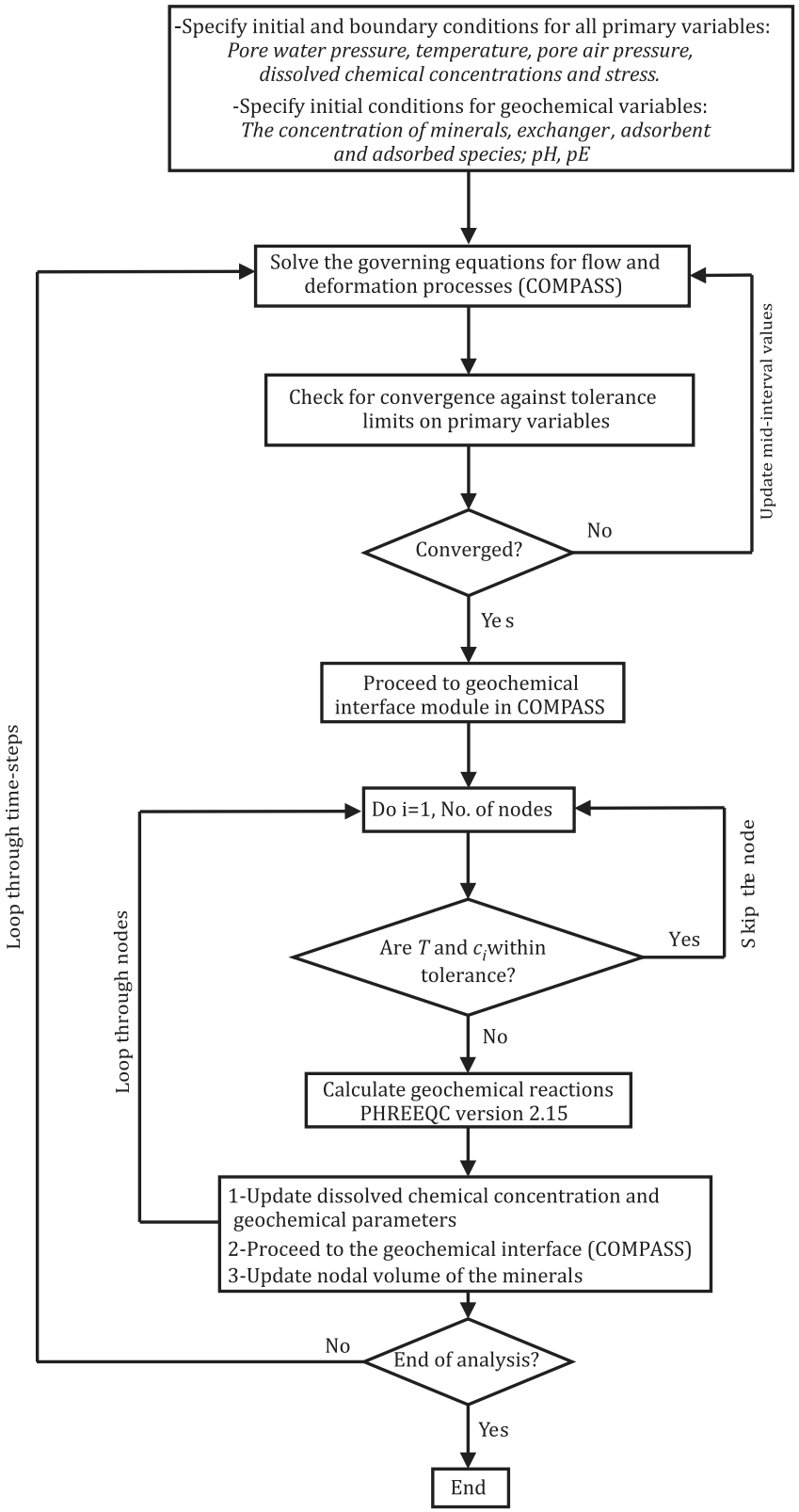

Fig. 15. Sequential noniterative approach (SNIA) adopted for coupling the transport model (COMPASS) and geochemical model (PHREEQC).

components where the diffusive flux no longer contains the mutual dependent concentration effects. Accordingly, a dependent ion is removed from the mass conservation in the transport model and its actual concentration is calculated by knowing the concentration of the remaining $(n_c - 1)$ components through the "no charge" condition $\sum_{i=1}^{n_c}[\partial(\theta_l z_i c_i \delta V)/\partial t] = 0$.

Appendix II. Numerical Formulation and Computational Approach

The governing differential equation for transport of an arbitrary chemical component in a coupled form with thermal, hydraulic, and chemical primary variable can be described as

$$C_{c_i l}\frac{\partial u_l}{\partial t}+C_{c_i T}\frac{\partial T}{\partial t}+C_{c_i a}\frac{\partial u_a}{\partial t}+C_{c_i}\frac{\partial c_i}{\partial t}=\nabla\cdot(K_{c_i l}\nabla u_l)$$
$$+\nabla\cdot(K_{c_i T}\nabla T)+\nabla\cdot(K_{c_i a}\nabla u_a)+\nabla\cdot\left(\sum_{j=1}^{n_c}K_{c_i c_j}\nabla c_j\right)+f_{c_i} \quad (24)$$

where C and K are lumped coefficients of the equation and f_{c_i} represents the chemical flux of the i^{th} component normal to the boundary surface.

The numerical solution of the formulations is achieved by the application of the finite element (in space) and the finite difference (in time) (Thomas and He 1998). The Galerkin weighted residual method is adopted by which the spatial discretization is developed and the residual error resulting from an approximate function over the entire element domain is minimized using the shape functions, given as

$$\int N_r R_\Omega d\Omega^e = 0 \quad (25)$$

where N_r is the shape function, R_Ω is the residual factor, and Ω^e represents the entire element domain.

Applying this method to the governing differential equation for an arbitrary chemical component in terms of the approximate functions yields

$$\int N_r\left[-C_{c_i l}\frac{\partial u_l}{\partial t}-C_{c_i T}\frac{\partial T}{\partial t}-C_{c_i a}\frac{\partial u_a}{\partial t}-C_{c_i}\frac{\partial c_i}{\partial t}+\nabla\cdot(K_{c_i T}\nabla T)\right.$$
$$\left.+\nabla\cdot(K_{c_i a}\nabla u_a)+\nabla\cdot\left(\sum_{j=1}^{n_c}K_{c_i c_j}\nabla c_j\right)+J_{c_i}\right]d\Omega^e=0 \quad (26)$$

The spatially discretized equations can then be combined and presented in a matrix form: (Thomas and He 1998):

$$\mathbf{K}\{\phi\}+\mathbf{C}\left\{\frac{\partial\phi}{\partial t}\right\}=\{f\} \quad (27)$$

where ϕ is the vector of primary variables (unknowns), $\mathbf{K}$ and $\mathbf{C}$ are the corresponding matrices of the governing equation, and f is the RHS vector and detailed elsewhere (Seetharam et al. 2007).

Details of the numerical solution to the coupled THM and THCM formulation of the model have been comprehensively discussed by Thomas and He (1998) and Seetharam et al. (2007).

The computational solution used for the reactive transport formulations is based on a time-splitting approach. The governing equations for the transport and the geochemical reactions are therefore solved sequentially. The coupling scheme adopted here between the transport model (COMPASS) and geochemical model (PHREEQC) is a sequential noniterative approach (SNIA). Fig. 15 presents the SNIA coupling approach and modular data exchange between COMPASS and PHREEQC.

The numerical formulation concerning reactive chemical equations by PHREEQC has been described elsewhere (Parkhurst and Appelo 1999). The model has been used with no alteration to its numerical formulation. In summary, there are two numerical solutions adopted in PHREEQC to solve problems involving multiple chemical reactions (Parkhurst and Appelo 1999):

1. A modified Newton-Raphson method is employed to solve a series of nonlinear algebraic equations for chemical reactions under equilibrium reactions.
2. For kinetically controlled reaction, the model uses a Runge-Kutta algorithm, which integrates the rate of reactions over time. The scheme includes a Runge-Kutta method with lower order to derive an error estimate with up to six intermediate evaluations of the derivative (Parkhurst and Appelo 1999).

Acknowledgments

The financial support received by the first author in the form of a PhD scholarship from the UK's Overseas Research Students Awards Scheme (ORSAS) is gratefully acknowledged. The support and contribution from Dr Suresh C. Seetharam (former Research Fellow at Cardiff University and currently a Scientist at the Belgian Nuclear Research Centre) in the early stages of this research is also gratefully acknowledged.

References

Agar, J. N., C. Y. Mou, and J. Lin. 1989. "Single-ion heat of transport in electrolyte solutions, A hydrodynamic theory." *J. Phys. Chem.* 93 (5): 2079–2082. https://doi.org/10.1021/j100342a073.

Arcos, D., F. Grandia, C. Domènech, A. M. Fernández, M. V. Villar, A. Muurinen, T. Carlsson, P. Sellin, and P. Hernán. 2008. "Long-term geochemical evolution of the near field repository: Insights from reactive transport modelling and experimental evidences." *J. Contam. Hydrol.* 102 (3–4): 196–209. https://doi.org/10.1016/j.jconhyd.2008.09.021.

Balluffi, R. W., S. M. Allen, and W. C. Carter 2005. *Kinetics of materials*. Hoboken, NJ: Wiley.

Boudreau, B. P., F. J. R. Meysman, and J. J. Middelburg. 2004. "Multicomponent ionic diffusion in pore water: Columbic effects revisited." *Earth Planetary Sci. Lett.* 222 (2): 653–666. https://doi.org/10.1016/j.epsl.2004.02.034.

Cleall, P. J., S. C. Seetharam, and H. R. Thomas. 2007. "On the inclusion of some aspects of chemical behaviour of an unsaturated soil in thermo-hydro-chemical-mechanical models. Part II: Application and transport of soluble salts in compacted bentonite." *J. Eng. Mech.* 133 (3): 348–356. https://doi.org/10.1061/(ASCE)0733-9399(2007)133:3(348).

Cuevas, J., M. V. Villar, M. Martín, J. C. Cobeña, and S. Leguey. 2002. "Thermo-hydraulic gradients on bentonite: Distribution of soluble salts, microstructure and modification of the hydraulic and mechanical behaviour." *Appl. Clay Sci.* 22 (1–2): 25–38. https://doi.org/10.1016/S0169-1317(02)00109-6.

Cussler, E. L. 1997. *Diffusion-mass transfer in fluid systems*. Cambridge, UK: Cambridge University Press.

ENRESA (Empresa Nacional de Residuos Radiactivos S.A.). 2000. *Full-scale engineered barriers experiment for a deep geological repository for high-level radioactive waste in crystalline host rock*. FEBEX project. EUR 19147. Luxembourg: Nuclear Science and Technology Series, European Communities.

Fernández, A. M., B. Baeyens, M. Bradbury, and P. Rivas. 2004. "Analysis of the pore water chemical composition of a Spanish compacted bentonite used in an engineered barrier." *Phys. Chem. Earth* 29: 105–118.

Fernández, A. M., J. Cuevas, and P. Rivas. 2001. "Pore water chemistry of the FEBEX bentonite." In Vol. 663 of *Proc., Material Research Society Symp.*, edited by K. P. Hart, G. R. Lumpkin, 573–588. Warrendale, PA: Materials Research Society.

Fernández, A. M., and M. V. Villar. 2010. "Geochemical behaviour of a bentonite barrier in the laboratory after up to 8 years of heating and hydration." *Appl. Geochem.* 25 (6): 809–824. https://doi.org/10.1016/j.apgeochem.2010.03.001.

García-Gutiérrez, M., J. L. Cormenzana, T. Missana, and M. Mingarro. 2004. "Diffusion coefficients and accessible porosity for HTO and 36Cl in compacted FEBEX bentonite." *Appl. Clay Sci.* 26 (1–4): 65–73. https://doi.org/10.1016/j.clay.2003.09.012.

Guimarães, L. D. N., A. Gens, and S. Olivella. 2007. "Coupled thermo-hydro-mechanical and chemical analysis of expansive clay subjected to heating and hydration." *Transp. Porous Media* 66 (3): 341–372. https://doi.org/10.1007/s11242-006-0014-z.

Holmboe, M., S. Wold, and M. Jonsson. 2012. "Porosity investigation of compacted bentonite using XRD profile modelling." *J. Contam.*

Hydrol. 128 (1–4): 19–32. https://doi.org/10.1016/j.jconhyd.2011.10.005.

Hueckel, T. A. 1992. "Water-mineral interaction in hydromechanics of clay exposed to environmental loads: A mixture-theory approach." *Can. Geotech. J.* 29 (6): 1071–1086. https://doi.org/10.1139/t92-124.

Jacques, D., and J. Šimůnek. 2005. *User manual of the multicomponent variably- saturated flow and transport model HP1. Description, verification, and examples*. BLG-998 Rep. Mol, Belgium: SCK·CEN.

Kozaki, T., K. Inada, S. Sato, and H. Ohashi. 2001. "Diffusion mechanism of chloride ions in sodium montmorillonite." *J. Contam. Hydrol.* 47 (2–4): 159–170. https://doi.org/10.1016/S0169-7722(00)00146-7.

Kröhn, K.-P. 2003. "New conceptual models for the resaturation of bentonite." *Appl. Clay Sci.* 23 (1–4): 25–33. https://doi.org/10.1016/S0169-1317(03)00083-8.

Laird, D. A. 2006. "Influence of layer charge on swelling of smectite." *Appl. Clay Sci.* 34 (1–4): 74–87. https://doi.org/10.1016/j.clay.2006.01.009.

Langmuir, D. 1997. *Aqueos environmental geochemistry.* Upper Saddle River, NJ: Prentice-Hall.

Lasaga, A. C. 1979. "The treatment of multicomponent diffusion and ion pairs in diagenetic fluxes." *Am. J. Sci.* 279 (3): 324–346. https://doi.org/10.2475/ajs.279.3.324.

Lasaga, A. C. 1981. "Reply-diffusion of seawater ions: Significance and consequences of cross coupling effects: Further comments and clarifications." *Am. J. Sci.* 281: 981–988.

Lasaga, A. C. 1998. "Kinetic theory in the earth science." *Princeton series in geochemistry.* Princeton, NJ: Princeton University Press.

Likos, W. J., and N. Lu. 2006. "Pore-scale analysis of bulk volume change from crystalline swelling in Na^{+2+} smectite." *Clays Clay Miner.* 54 (4): 515–528. https://doi.org/10.1346/CCMN.2006.0540412.

Likos, W. J., and A. Wayllace. 2010. "Porosity evolution of free and confined bentonite during interlayer hydration." *Clays Clay Miner.* 58 (3): 399–414. https://doi.org/10.1346/CCMN.2010.0580310.

Martín, M., J. Cuevas, and S. Leguey. 2000. "Diffusion of soluble salts under a temperature gradient after the hydration of compacted bentonite." *Appl. Clay Sci.* 17 (1–2): 55–70. https://doi.org/10.1016/S0169-1317(00)00006-5.

Mayhew, Y. R., and G. F. C. Rogers. 1976. *Thermodynamic and transport properties of fluids*. 2nd ed. Oxford: Blackwell.

Muurinen, A., O. Karnland, and J. Lehikoinen. 2007. "Effect of homogenization on the microstructure and exclusion of chloride in compacted bentonite." *Phys. Chem. Earth* 32 (1–7): 485–490. https://doi.org/10.1016/j.pce.2006.02.058.

Navarro, V., L. Asensio, Á. Yustres, X. Pintado, and J. Alonso. 2014. "An elastoplastic model of bentonite free swelling." *Eng. Geol.* 181: 190–201. https://doi.org/10.1016/j.enggeo.2014.07.014.

Oelkers, E. H. 1996. "Physical and chemical properties of rocks and fluids form chemical mass transport calculations." *React. Transp. Porous Media Rev. Min.* 34 (1): 130–191.

Parkhurst, D. L., and C. A. J. Appelo. 1999. *User's guide to PHREEQC (version 2)*. Water Resource Investigation Rep. Reston, VA: US Geological Survey.

Philip, J. R., and D. A. de Vries. 1957. "Moisture movement in porous materials under temperature gradients." *Trans. Am. Geophys. Union* 38 (2): 222–232. https://doi.org/10.1029/TR038i002p00222.

Pusch, R., O. Karnland, and H. Hokmark. 1990. *GMM: A general microstructural model for qualitative and quantitative studies of smectite clays, SKB*. Technical Rep. No. SKB-90-43. Stockholm, Sweden: Swedish Nuclear Fuel and Waste Management Company.

Pusch, R., and R. N. Yong. 2006. *Microstructure of smectite clays and engineering performance*. New York: Taylor & Francis.

Ransom, B., and H. C. Helgeson. 1994. "A chemical and thermodynamic model of aluminous dioctahedral 2:1 layer clay minerals in diagnetic processes: Regular solution representation of interlayer dehydration in smectite." *Am. J. Sci.* 294 (4): 449–484. https://doi.org/10.2475/ajs.294.4.449.

Ransom, B., and H. C. Helgeson. 1995. "A chemical and thermodynamic model of aluminous dioctahedral 2:1 layer clay minerals in diagnetic processes: Dehydration of dioctahedral aluminous smectites as a function of temperature and depth in sedimentary." *Am. J. Sci.* 295 (3): 245–281. https://doi.org/10.2475/ajs.295.3.245.

Revil, A., and D. Jougnot. 2008. "Diffusion of ions in unsaturated porous materials." *J. Colloid Interface Sci.* 319 (1): 226–235. https://doi.org/10.1016/j.jcis.2007.10.041.

Samper, J., T. Xu, and C. Yang. 2009. "A sequential partly iterative approach for multicomponent reactive transport with CORE2D." *Comput. Geosci.* 13 (3): 301–316. https://doi.org/10.1007/s10596-008-9119-5.

Samper, J., L. Zheng, L. Montenegro, A. M. Fernández, and P. Rivas. 2008. "Testing coupled thermo-hydro-chemical models of compacted bentonite after dismantling the FEBEX in situ test." *Appl. Geochem.* 23 (5): 1186–1201. https://doi.org/10.1016/j.apgeochem.2007.11.010.

Sánchez, M., A. Gens, and S. Olivella. 2012. "THM analysis of a large-scale heating test incorporating material fabric changes." *Int. J. Numer. Anal. Methods Geomech.* 36 (4): 391–421. https://doi.org/10.1002/nag.1011.

Sedighi, M. 2011. "An investigation of hydro-geochemical processes in coupled thermal, hydraulic, chemical and mechanical behaviour of unsaturated soils." Ph.D. thesis. Cardiff Univ. http://orca.cf.ac.uk/54236/1/U573143.pdf.

Sedighi, M., and H. R. Thomas. 2014. "Micro porosity evolution in compacted swelling clays—A chemical approach." *Appl. Clay Sci.* 101: 608–618. https://doi.org/10.1016/j.clay.2014.09.027.

Sedighi, M., H. R. Thomas, S. A. Masum, P. J. Vardon, D. Nicholson, and Q. Chen. 2015. "Geochemical modelling of hydrogen gas migration in an unsaturated bentonite buffer." *Geol. Soc. J.* 415 (1): 189–201. https://doi.org/10.1144/SP415.12.

Sedighi, M., H. R. Thomas, and P. J. Vardon. 2011. "Modelling thermal impacts on reactive transport processes related to multicomponent chemicals in compacted clays." In *Proc., 2nd Int. Symp. on Computational Geomechanics (ComGeo II)*, 538–546. Rhodes, Greece: International Centre of Computational Engineering.

Sedighi, M., H. R. Thomas, and P. J. Vardon. 2016. "Reactive transport of chemicals in unsaturated soils: Numerical model development and verification." *Can. Geotech. J.* 53 (1): 162–172. https://doi.org/10.1139/cgj-2014-0436.

Seetharam, S. C., H. R. Thomas, and P. J. Cleall. 2007. "Coupled thermo-hydrochemical- mechanical model for unsaturated soils-numerical algorithm." *Int. J. Numer. Methods Eng.* 70 (12): 1480–1511. https://doi.org/10.1002/nme.1934.

Steefel, C. I. 1996. "Approaches to modeling of reactive transport in porous media." In Vol. 34 of *Reactive transport in porous media, reviews in mineralogy.* Washington, DC: Mineralogical Society of America.

Steefel, C. I. 2009. "CrunchFlow software for modeling multicomponent reactive flow and transport, user's manual." Lawrence Berkeley National Laboratory. https://www.netl.doe.gov/File%20Library/Research/Oil-Gas/methane%20hydrates/CrunchFlow-Manual.pdf.

Steefel, C. I., J. Rutqvist, C.-F. Tsang, H.-H. Liu, E. Sonnenthal, J. Houseworth, and J. Birkholzer. 2010. *Reactive transport and coupled THM processes in engineering barrier systems (EBS).* Technical Rep. No. LBNL-3901E. Berkeley, CA, Lawrence Berkeley National Laboratory.

Thomas, H. R., P. J. Cleall, N. Chandler, D. Dixon, and H. P. Mitchell. 2003. "Water infiltration into a large-scale in-situ experiment in an underground research laboratory." *Géotechnique* 53 (2): 207–224. https://doi.org/10.1680/geot.2003.53.2.207.

Thomas, H. R., and Y. He. 1997. "A coupled heat–moisture transfer theory for deformable unsaturated soil and its algorithmic implementation." *Int. J. Numer. Methods Eng.* 40 (18): 3421–3441. https://doi.org/10.1002/(SICI)1097-0207(19970930)40:18<3421::AID-NME220>3.0.CO;2-C.

Thomas, H. R., and Y. He 1998. "Modelling the behaviour of unsaturated soil using an elasto plastic constitutive relationship." *Géotechnique* 48: 589–603.

Thomas, H. R., and M. Sedighi. 2012. "Modelling the engineering behaviour of highly swelling clays." In *Proc., 4th International Conference on Problematic Soils*, 21–33. Singapore: Ci-Premier PTE Limited.

Thomas, H. R., M. Sedighi, and P. J. Vardon. 2012. "Diffusive reactive transport of multicomponent chemicals under coupled thermal,

hydraulic, chemical and mechanical conditions." *Geotech. Geol. Eng.* 30 (4): 841–857. https://doi.org/10.1007/s10706-012-9502-9.

Van Genuchten, M. 1980. "A closed-form equation for predicting the hydraulic conductivity of unsaturated soils." *Soil Sci. Soc. Am. J.* 44 (5): 892–898. https://doi.org/10.2136/sssaj1980.03615995004400050002x.

Van Loon, L. R., M. A. Glaus, and W. Müller. 2007. "Anion exclusion effects in compacted bentonite: Towards a better understanding of anion diffusion." *Appl. Geochem.* 22 (11): 2536–2552. https://doi.org/10.1016/j.apgeochem.2007.07.008.

Vardon, P. J., P. J. Cleall, H. R. Thomas, R. N. Philp, and I. Banicescu. 2011. "Three-dimensional field-scale coupled thermo-hydro-mechanical modelling: A parallel computing implementation." *Int. J. Geomech.* 11 (2): 90–98. https://doi.org/10.1061/(ASCE)GM.1943-5622.0000019.

Vidal, O., and B. Dubacq. 2009. "Thermodynamic modelling of clay dehydration, stability and compositional evolution with temperature, pressure and H_2O activity." *Geochim. Cosmochim. Acta* 73 (21): 6544–6564. https://doi.org/10.1016/j.gca.2009.07.035.

Villar, M. V. 2007. "Water retention of two natural compacted bentonites." *Clays Clay Miner.* 55 (3): 311–322. https://doi.org/10.1346/CCMN.2007.0550307.

Villar, M. V., A. M. Fernández, P. L. Martín, J. M. Barcala, R. Gómez-Espina, and P. Rivas. 2008a. *Effect of heating/hydration on compacted bentonite: Tests in 60 cm long cells*. Madrid, Spain: Publishing House CIEMAT.

Villar, M. V., M. Sánchez, and A. Gens. 2008b. "Behaviour of a bentonite barrier in the laboratory: Experimental results up to 8 years and numerical simulation." Supplement, *Phys. Chem. Earth* 33 (S1) : S476–S485. https://doi.org/10.1016/j.pce.2008.10.055.

Warr, L., and J. Berger. 2007. "Hydration of bentonite in natural waters: Application of 'confined volume' wet-cell X-ray diffractometry." *Phys. Chem. Earth A/B/C* 32 (1–7): 247–258. https://doi.org/10.1016/j.pce.2006.02.048.

Wersin, P., E. Curti, and C. A. J. Appelo. 2004. "Modelling bentonite-water interaction at high solid/liquid ratios: Swelling and diffuse double layer effects." *Appl. Clay Sci.* 26 (1–4): 249–257. https://doi.org/10.1016/j.clay.2003.12.010.

Xie, M., S. Bauer, O. Kolditz, T. Nowak, and H. Shao. 2006. "Numerical simulation of reactive processes in an experiment with partially saturated bentonite." *J. Contam. Hydrol.* 83 (1–2): 122–147. https://doi.org/10.1016/j.jconhyd.2005.11.003.

Xu, T., E. Sonnenthal, N. Spycher, and K. Pruess. 2004. "TOURGHREACT: A simulation program for non-isothermal multiphase reactive geochemical transport in variably saturated geologic media." *Comp. Geosci.* 32 (2): 145–165.

Yang, C., J. Samper, and L. Montenegro. 2008. "A coupled non-isothermal reactive transport model for long-term geochemical evolution of a HLW repository in clay." *Environ. Geol.* 53 (8): 1627–1638. https://doi.org/10.1007/s00254-007-0770-2.

Yeh, G. T., and V. S. Tripathi. 1989. "A critical evaluation of recent developments in hydrogeochemical transport models of reactive multichemical components." *Water Resour. Res.* 25 (1): 93–108. https://doi.org/10.1029/WR025i001p00093.

Yong, R. N. 2003. "Influence of microstructural features on water, ion diffusion and transport in clay soils." *Appl. Clay Sci.* 23 (1–4): 3–13. https://doi.org/10.1016/S0169-1317(03)00081-4.

Zagorščak, R., M. Sedighi, and H. R. Thomas. 2017. "Effects of thermo-osmosis on hydraulic behavior of saturated clays." *Int. J. Geomech.* 17 (3): 04016068. https://doi.org/10.1061/(ASCE)GM.1943-5622.0000742.

Zheng, L., and J. Samper. 2008. "Coupled THMC model of FEBEX mock-up test." Supplement, *Phys. Chem. Earth* 33 (S1) : S486–S498. https://doi.org/10.1016/j.pce.2008.10.023.